# Spectral shapes of the fluxes of electrons and positrons and the average residence time of cosmic rays in the Galaxy

Paolo Lipari*

*INFN, Sezione Roma "Sapienza," piazzale Aldo Moro 2, 00185 Roma, Italy*

(Received 7 October 2018; published 12 February 2019)

The cosmic ray energy spectra encode very important information about the mechanisms that generate relativistic particles in the Milky Way, and about the properties of the Galaxy that control their propagation. Relativistic electrons and positrons traveling in interstellar space lose energy much more rapidly than more massive particles such as protons and nuclei, with a rate that grows quadratically with the particle energy $E$. One therefore expects that the effects of energy loss should leave observable signatures in the $e^{\mp}$ spectra, in the form of softenings centered at the critical energy $E^{*}$. This quantity is determined by the condition that the total energy loss suffered by particles during their residence time in the Galaxy is of the same order as the initial energy. If the electrons and positrons are accelerated in discrete (quasi) pointlike astrophysical objects, such as supernova explosions or pulsars, the stochastic nature of the sources should also leave observable signatures in the $e^{\mp}$ energy spectra and angular distributions above a second (higher) critical energy $E^{\dagger}$, determined by the condition that particles with $E \gtrsim E^{\dagger}$ can propagate only for a maximum distance shorter than the average separation between sources. In this work we discuss the theoretically expectations for the signatures of the energy-loss effects on the electron and positron spectra, and compare these predictions with the existing observations. Recent measurements of the $(e^{-} + e^{+})$ flux have discovered the existence of a prominent spectral break at $E \simeq 1$ TeV. This spectral feature can perhaps be identified with the critical energy $E^{*}$. An alternative hypothesis is to assume that $E^{*}$ has a much lower value of order of a few GeV. Resolving this ambiguity is of great importance for our understanding of Galactic cosmic rays.

DOI: 10.1103/PhysRevD.99.043005

## I. INTRODUCTION

The fluxes of cosmic rays (CR) that are observable near the Earth, in a very broad energy interval that extends from GeV's to PeV's (and possibly to much higher energy), are formed by particles of Galactic origin. These CR particles are injected in interstellar space by sources distributed in the entire Milky Way and remain confined in the Galaxy for an extended period of time because of the existence of the Galactic magnetic fields. The CR fluxes are, to a very good approximation, isotropic, but their energy distributions contain very important information about their sources and about the properties of the Galaxy that control CR propagation. At low energy ($E \lesssim 30$ GeV) the CR spectra are also distorted by the electromagnetic fields that fill the heliosphere, generating time-dependent solar modulations.

A fundamental problem for CR astrophysics is to disentangle the roles of the sources and of propagation in the formation of the CR fluxes, reconstructing the "source spectra" (that is, the spectra with which the particles are injected in interstellar space by the sources) from the observations, and the distortion effects generated by propagation.

Relativistic, electrically charged particles propagating in interstellar space continuously lose energy because of different types of interactions. The rate of energy loss (for particles of the same $E$) is however many orders of magnitude larger for particles of small mass (with the dominant mechanisms scaling $\propto m^{-4}$). It is therefore expected that the energy-loss effects play a significant role only in the propagation of electrons and positrons, and that they are entirely negligible in the propagation of $p$, $\bar{p}$ and nuclei.

The rate of energy loss for $e^{\mp}$ also grows rapidly with the particle energy (in good approximation $\propto E^{2}$), so the effects of energy losses are significant only for particles of sufficiently high $E$. The conclusion is that the spectra of both the $e^{-}$ and $e^{+}$ fluxes should exhibit the "imprint" of the energy losses in the form of a softening feature that marks the transition from a regime where energy losses are negligible ($E \lesssim E^{*}$) to a regime where energy losses are the most important "sink" that balances the injection of new particles by the sources ($E \gtrsim E^{*}$). The identification of the softening features in the $e^{\mp}$ spectra allows a measurement of the critical energy $E^{*}$.

The physical condition that determines $E^{*}$ is that the total energy lost by a particle injected in interstellar space with initial energy $E^{*}$, calculated by integrating the loss rate

*paolo.lipari@roma1.infn.it

 

during the time interval when the particle remains confined in the Galaxy, is (on average) of the same order of magnitude. This condition can be expressed in the form

$$\langle \Delta E(E^*) \rangle = \langle dE/dt(E^*) \rangle T_{\rm esc}(E^*) \approx E^*. \qquad (1)$$

In this equation $\langle dE/dt(E) \rangle$ is the rate of energy loss averaged over the CR confinement volume, and $T_{\rm esc}(E)$ is the average residence time of a particle of initial energy $E$. The crucially important point is that the identification of the critical energy $E^*$ allows a measurement of the residence time of CR in the Galaxy, a quantity of fundamental importance for our understanding of cosmic rays.

In the discussion above we have implicitly assumed that the critical energies for electrons and positrons $E^*_{e^-}$ and $E^*_{e^+}$ are approximately equal. This is a simple and robust prediction that can be used to test the hypothesis that a spectral feature observed in the spectrum of one particle type is indeed generated by energy-loss effects. If this is the case, a softening feature of approximately the same structure, and centered at approximately the same energy, must also be present in the spectrum of the other particle type. It should, however, be noted that the two critical energies for electrons and positrons are not exactly identical. The rates of energy loss for $e^+$ and $e^-$ in interstellar space are to a very good approximation equal, and the annihilation probability for CR positrons interacting with the electrons of the medium is negligibly small; however, the critical energy also depends on the space distributions of the CR sources, which can be different for the two particle types. In addition, one should take into account the fact that the spectral distortion generated by the energy losses depends on the shape of the source spectrum, which again is different for the two particle types.

When energy losses become important for the propagation of electrons and positrons, the space-time volume that contains sources that can contribute to the observed spectra starts to shrink rapidly for increasing $E$. If the CR sources are discrete and transient astrophysical objects, the reduction in the space-time volume for the CR sources corresponds to a smaller number of astrophysical objects that can contribute to the flux. When this number becomes sufficiently small, the "granularity" (or "stochasticity") of the sources should become observable as an anisotropy in the angular distribution of the flux and/or in additional features in the energy spectra. The search for these predicted source granularity effects is an important task in the study of the $e^{\mp}$ spectra.

This work is organized as follows: In the next section we discuss the observations of the $e^-$, $e^+$ and $(e^- + e^+)$ spectra, fitting the data with simple functional forms. Section III discusses theoretical models for the formation of the Galactic CR spectra. In this discussion we introduce two very simple models for Galactic propagation, where the CR propagation can be expressed with exact analytic expressions. The first one is the "leaky box" model; the second one is a diffusion model that gives results that are very close to those that can be obtained numerically with computer codes such as GALPROP or DRAGON. These models should only be considered as first-order approximations to a realistic description of CR propagation, but they can be used as a qualitative (or semiquantitative) guide to the expected spectral shapes for different particle types. The diffusion model also allows us to study the size and shape of the space region where the CR particles have been produced. In Sec. IV we assume that CR are generated in "source events" (such as supernovae explosions) that are pointlike and instantaneous and, using the framework of the diffusion model, compute how the observed flux is formed by the contributions of different source events and how the granularity of the source could become observable. Section V discusses how the theoretical models compare to the observations. We argue that there are two possible solutions for the critical energy $E^*$ ($E^* \sim 3$ GeV) or $E^* \simeq 1$ TeV. These two solutions have profoundly different implications for cosmic ray astrophysics, as discussed in Sec. VI. A final section gives a summary and an outlook for future studies.

## II. OBSERVATIONS

The spectra of CR electrons and positrons have been measured with good accuracy by the magnetic spectrometers PAMELA [1–5] and AMS02 [6,7] for $E \lesssim 500$ GeV (see Figs. 1 and 2). The two detectors have taken data during nonoverlapping time intervals, and the large differences in flux observed for $E \lesssim 20$ GeV can be attributed to time variations associated with the effects of (time-dependent) solar modulations that distort a (constant) interstellar spectrum.

In the discussion of the CR energy distributions, it is useful to consider the (energy-dependent) spectral index

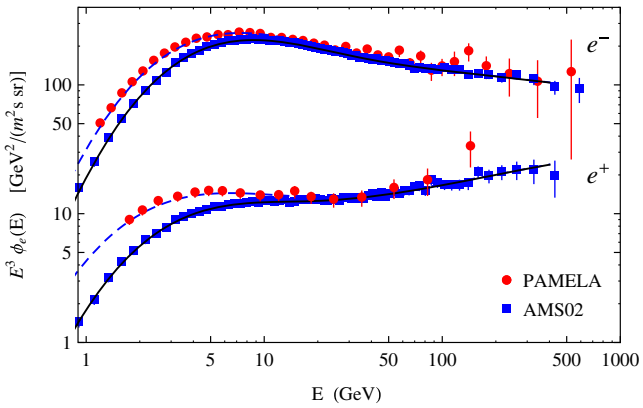


FIG. 1. Spectra of $e^{\mp}$ measured by PAMELA [1,2] (squares) and AMS02 [6] (circles) shown in the form $E^3\phi_{e^{\mp}}(E)$ versus $E$. The energy scale of the PAMELA has been rescaled by a factor $f = 0.93$. The lines are fit to the data discussed in the text.

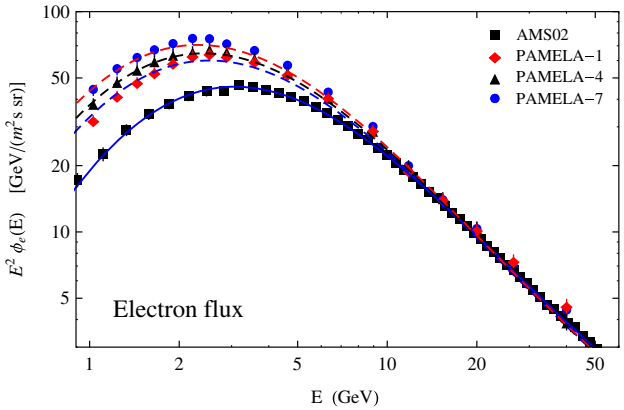


FIG. 2. Electron spectra measured by AMS02 [6] and by PAMELA [4] in different time intervals. The energy scale of PAMELA has been rescaled by a factor $f = 0.93$. The lines are fit to the data discussed in the main text.

$\gamma(E)$, which is the slope of the spectrum when shown in the form $\log\phi$ versus $\log E$:

$$\gamma(E) = -\frac{d\log\phi}{d\log E} = -\frac{E}{\phi}\frac{d\phi}{dE}. \tag{2}$$

The energy spectra of both electrons and positrons have the following qualitative properties.

(i) For $E \lesssim 20$ GeV (which is also the region where time-dependent solar modulations are important) the spectra exhibit a strong curvature and soften gradually, as the spectral indices $\gamma_{e^\mp}(E)$ grow continuously with energy.

(ii) At high energy ($E \gtrsim 50$ GeV) the spectra can be well fitted with simple power laws, and the spectral indices are approximately constant (with values $\gamma_{e^-} \simeq 3.17$ and $\gamma_{e^+} \simeq 2.74$).

(iii) The spectral indices of both electrons and positrons have a maximum at an energy of order 20 GeV (more accurately, $E \simeq 24$ GeV for electrons and $E \simeq 14$ GeV for positrons). This implies that both spectra undergo a modest, but clearly visible hardening for energy around 10–30 GeV.

To describe the data we use a simple model where the interstellar spectra have a broken power-law form (with one hardening), and the solar modulations are described by the force field approximation (FFA) [8]. A convenient expression to describe a spectrum with one gradual break (see [9] for a more detailed discussion) is

$$\phi_0(E) = K_0\left(\frac{E}{E_0}\right)^{-\gamma_1}\left[1+\left(\frac{E}{E_b}\right)^{\frac{1}{w}}\right]^{-(\gamma_2-\gamma_1)w}. \tag{3}$$

This five-parameter expression (with $E_0$ an arbitrary reference energy that, in this work, will be fixed at 10 GeV) describes a spectrum that is asymptotically (at low and high energy) a simple power law with slopes $\gamma_1$ and $\gamma_2$. At the break energy $E_b$ the spectral index takes the average value $\gamma(E_b) = (\gamma_1+\gamma_2)/2$, and $w$ gives the width of the interval in $\log E$ where the spectral index varies.

In the FFA [8] the effects of solar modulations are modeled as the loss of a constant energy $\Delta E = \varepsilon$ for all particles that traverse the heliosphere and reach the Earth. Making use of the Liouville theorem, and assuming that the CR flux is isotropic at the boundary of the heliosphere, one can derive the relation between the spectrum $\phi(E)$ observed at the Earth and the interstellar spectrum $\phi_0(E)$ (present at the boundary of the heliosphere):

$$\phi(E) = \frac{p^2}{p_0^2}\phi_0(E+\varepsilon) \tag{4}$$

where $p$ and $p_0$ are the momenta that correspond to the energies $E$ and $E_0 = E+\varepsilon$.

Observations of the time dependence of CR fluxes [5,7] clearly show that the solar modulation effects are different for positively and negatively charged particles. This can be understood (see e.g., [10] and references therein) as the effect of the large-scale heliospheric magnetic fields. Particles with electric charge of different sign travel along different trajectories and therefore, on average, can lose different amounts of energy. Accordingly, one expects that the parameter $\varepsilon$ will be different for electrons and positrons.

Applying the FFA algorithm to a spectrum of the form of Eq. (3), and considering ultrarelativistic electrons (so that $p \simeq E$ and $p_0 \simeq E_0$), one arrives at the (six-parameter) expression:

$$\phi(E) = K_0\frac{E^2}{(E+\varepsilon)^2}\left(\frac{E+\varepsilon}{E_0}\right)^{-\gamma_1}\left[1+\left(\frac{E+\varepsilon}{E_b}\right)^{1/w}\right]^{-(\gamma_2-\gamma_1)w}. \tag{5}$$

The expression of Eq. (5) can describe well the AMS02 data (taken between May 2011 and November 2013) for both electrons and positrons in the energy range $E >$ 1 GeV. The minimum $\chi^2$ (calculated by quadratically combining statistical and systematic errors) are $\chi^2_{\rm min} = 11.7$ (64 d.o.f.) for the electrons and $\chi^2_{\rm min} = 21.0$ (63 d.o.f.) for the positrons [11]. The results are shown in Fig. 1, and the best-fit parameters, with $1\sigma$ uncertainties, are listed in Table I.

The PAMELA Collaboration has published spectra of electrons [1] and positrons [2], taken in the time interval from January 2006 to December 2009. In the framework we have adopted here, the data taken in different time intervals should be fitted with the same expression used for AMS02, only changing the (time-dependent) parameter $\varepsilon$ in Eq. (5). However, we also allow for the possibility that the energy scales of the two experiments are different. Following these ideas we have studied the hypothesis that the PAMELA measurements of the $e^\mp$ spectra can be

TABLE I. Parameters of best fits to the AMS02 data on the electron and positron spectra [6] (in the range $E > 1$ GeV), using the functional form of Eq. (5). The $\chi^2$ of the fit is calculated by quadratically combining the stated statistical and systematic errors. The best-fit spectra are shown in Fig. 1.

| Particle | Electrons | Positrons |
|---|---|---|
| $K$ [GeV m$^2$ s sr]$^{-1}$ | $0.47^{+0.02}_{-0.03}$ | $0.018^{+0.0012}_{-0.003}$ |
| $\gamma_1$ | $3.89^{+0.27}_{-0.12}$ | $3.62^{+0.36}_{-0.22}$ |
| $\gamma_2$ | $3.17^{+0.05}_{-0.09}$ | $2.74^{+0.05}_{-0.15}$ |
| $E_b$ [GeV] | $32.9^{+5.3}_{-7.2}$ | $20.8^{+5.3}_{-12.4}$ |
| $w$ | $0.50^{+0.25}_{-0.15}$ | $0.55^{+0.29}_{-0.21}$ |
| $\varepsilon$ [GeV] | $1.44^{+0.31}_{-0.10}$ | $0.94^{+0.36}_{-0.14}$ |
| $\chi^2_{\rm min}$ | 11.7 | 21.0 |
| $N_{\rm d.o.f.}$ | 64 | 63 |

described by the same best-fit functions $\phi^{\rm AMS}_{e^\mp}(E)$, with a rescaling of the energy and the distortion due to a difference in the parameter $\varepsilon$.

This corresponds to fitting the PAMELA data from [1,2] with an expression that depends on two parameters. One parameter is the ratio between the scales of energy for the two detectors $f = E_{\rm AMS}/E_{\rm PAM}$. The second one is the quantity $\Delta\varepsilon = \varepsilon_{\rm PAM} - \varepsilon_{\rm AMS}$, which is the difference between the solar modulation parameters for the two data-taking time intervals.

This procedure yields best fits of reasonably good quality (in the energy range $E > 1$ GeV). For the electron spectrum one has $\chi^2_{\rm min} = 26.2$ (for 37 d.o.f.), while for the positron flux one has $\chi^2_{\rm min} = 4.8$ for 15 d.o.f.

The parameters of the best fit are given in Table II. The best-fit value for the parameter $\Delta\varepsilon$ is $-210 \pm 10$ MeV for electrons and $-280 \pm 20$ MeV for positrons. The best-fit values for the parameters $f_{e^\mp}$ show significant deviations from unity ($f_{e^-} \simeq 0.93 \pm 0.01$ and $f_{e^+} \simeq 0.94 \pm 0.02$). It is encouraging that these two values are consistent with being equal to each other and the deviations from unity (of 6% and 7%) are within the estimated systematic uncertainties on the energy scale for the two detectors [12]. It should also be noted that a review of the PAMELA data [3] discusses a revision of the normalization of the published data, in the same direction we find in the fit procedure.

TABLE II. Parameters of fits to the PAMELA data on the electron [1] and positron [2] fluxes. The data are fitted using the best-fit function obtained for the AMS data, assuming a constant energy rescaling factor $f = E_{\rm PAM}/E_{\rm AMS}$ and a difference in the FFA modulation parameter $\Delta\varepsilon = \varepsilon_{\rm PAM} - \varepsilon_{\rm AMS}$.

| Particle | Electrons | Positrons |
|---|---|---|
| $f$ | $0.93 \pm 0.01$ | $0.94 \pm 0.02$ |
| $\Delta\varepsilon$ [GeV] | $-0.21 \pm 0.01$ | $-0.28 \pm 0.02$ |
| $\chi^2_{\rm min}$ | 26.2 | 4.8 |
| $N_{\rm d.o.f.}$ | 37 | 15 |

These fits to the PAMELA data are shown in Fig. 1. [Note that in the figure the PAMELA data points (plotted together with the AMS02 data) show the energy rescaled by a factor 0.93.]

The PAMELA Collaboration has also published the results of seven measurements of the electron flux taken during separate six-month time intervals between July 2006 and December 2009 [4]. These results are limited to the lower energy region ($E \lesssim 50$ GeV) but are sufficient to obtain important information on the time dependence of the $e^-$ flux. These spectra have also been successfully fitted ($\chi^2_{\rm min}$ is in the range 1.0–8.3 for 14 d.o.f.) with the two-parameter model discussed above. The fits are shown in Fig. 2, and the best fits for the parameters $\{f, \Delta\varepsilon\}$ are listed in Table III. The energy rescale parameter in the different fits is consistent with being equal for all data sets $f \simeq 0.97$. The solar modulation-dependent parameter $\Delta\varepsilon$ takes values between $-200$ and $-310$ MeV.

More recently, the AMS02 Collaboration published [7] spectra of electrons and positrons in the energy range 1–50 GeV averaged during 79 time separate time intervals of 27 days. The FFA model for the solar modulations cannot reproduce these precisely measured spectra exactly; however, in a reasonably good first approximation, it still gives a good description of the data, as shown in Fig. 3. A more detailed study of this problem is postponed to a future work.

### A. The $(e^- + e^+)$ spectrum

Calorimetric measurements of the sum of electrons and positrons, performed without separating the two particle types, are shown in Figs. 4 and 5. Direct observations of this spectrum have been performed by AMS02 [13], FERMI [14], ATIC [15], CALET [16,17], and DAMPE [18]. These measurements reach (in the case of DAMPE) a maximum energy $E \simeq 4.5$ TeV.

Ground-based Cherenkov telescopes such as HESS [19,20], MAGIC [22], and VERITAS [23] have also been

TABLE III. Parameters of fits to the electron PAMELA taken during different time intervals [4]. The data are fitted using the best-fit function obtained for the AMS data, assuming a constant energy rescaling factor $f = E_{\rm PAM}/E_{\rm AMS}$ and a difference in the FFA modulation parameter $\Delta\varepsilon = \varepsilon_{\rm PAM} - \varepsilon_{\rm AMS}$.

| Data set | Time | $f$ | $\Delta\varepsilon$ | $\chi^2_{\rm min}$ |
|---|---|---|---|---|
| 1 | Jul–Nov 2006 | $0.975 \pm 0.013$ | $-0.208 \pm 0.013$ | 7.7 |
| 2 | Jan–Jun 2007 | $0.974 \pm 0.012$ | $-0.243 \pm 0.012$ | 3.9 |
| 3 | Jul–Dec 2007 | $0.967 \pm 0.012$ | $-0.256 \pm 0.012$ | 8.3 |
| 4 | Jan–Jun 2008 | $0.960 \pm 0.013$ | $-0.259 \pm 0.012$ | 1.0 |
| 5 | Jul–Dec 2008 | $0.962 \pm 0.014$ | $-0.284 \pm 0.012$ | 2.7 |
| 6 | Jan–Jun 2009 | $0.956 \pm 0.014$ | $-0.310 \pm 0.013$ | 3.2 |
| 7 | Jul–Dec 2009 | $0.976 \pm 0.018$ | $-0.307 \pm 0.014$ | 5.6 |

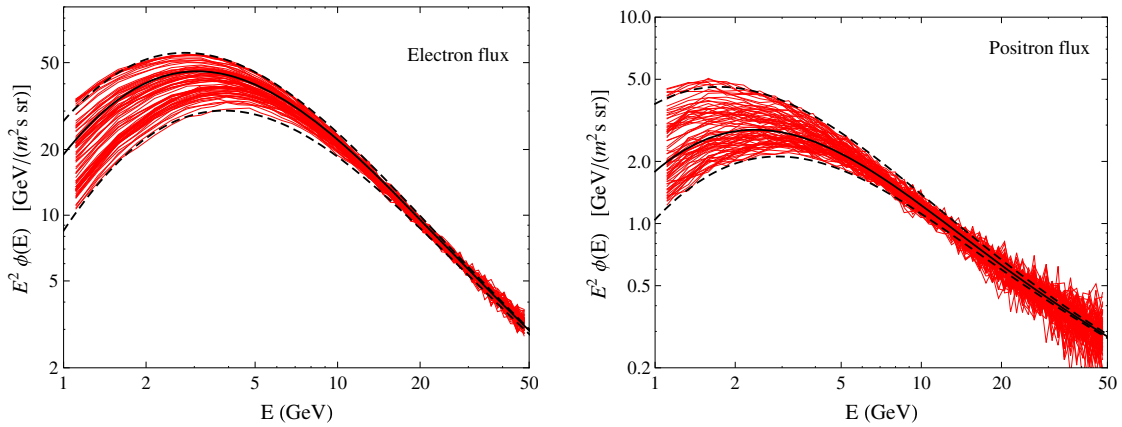


FIG. 3. Measurements of the electron (left panel) and positron (right panel) spectra taken during 79 different time intervals (of 27 days) by the AMS02 Collaboration [7]. The thick solid lines are the fits of the time-averaged $e^{\mp}$ spectra discussed in this work. The dashed lines are calculated by distorting the average spectra using the FFA model for solar modulations with different parameters.

able to obtain measurements of the $(e^- + e^+)$ spectrum in the TeV energy range. The measurements are performed by selecting events that are consistent with an electromagnetic shower and subtracting the background generated by cosmic ray protons and nuclei using Monte Carlo codes to model the developments of air showers. Recently, the HESS telescope [21] presented measurements of the spectrum that extend to $E \simeq 20$ TeV.

The observations of ATIC [15] show a surprising structure in the spectrum at an energy of 700 GeV, which has been the object of many efforts at interpretation, generating a large body of literature. However, the existence of this structure has not been confirmed by the measurements of FERMI, DAMPE, HESS, and the other Cherenkov detectors, and in the present work it is considered as the consequence of some unaccounted for systematic effects.

The data of the other experiments are not in perfect agreement with each other; e.g., (see Fig. 5), the measurements of DAMPE and HESS differ by approximately 25%–30% in the energy range 500–1000 GeV. The observations, however, clearly show the existence of a remarkable spectral break at $E \approx 1$ TeV.

The existence of this spectral feature was first discovered by the HESS Collaboration [20], confirmed by MAGIC [22] and VERITAS [23], and then also clearly seen by the DAMPE detector [18]. The results of FERMI [14] are actually consistent with an unbroken power-law spectrum, but the errors of the highest energy points, which reach 2 TeV, are large, and this does not appear to be a significant discrepancy.

The HESS Collaboration [21] has presented a fit to their more recent data with the same expression

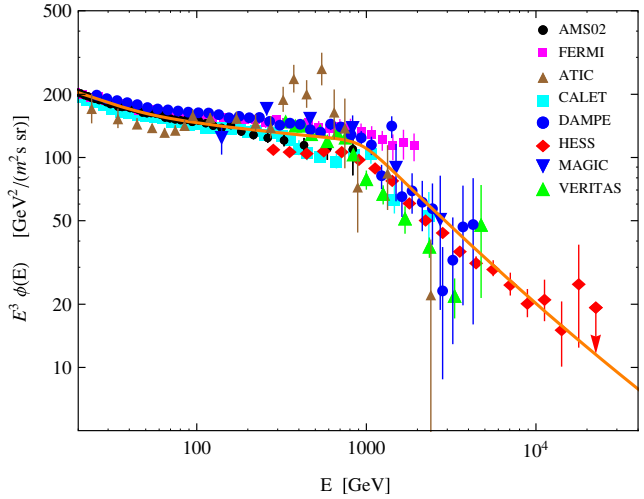


FIG. 4. Measurements of the $(e^- + e^+)$ spectrum obtained by AMS02 [13], FERMI [14], ATIC [15], CALET [16,17], DAMPE [18], HESS [19–21], MAGIC [22], and VERITAS [23]. The line is a fit to the data from [24].

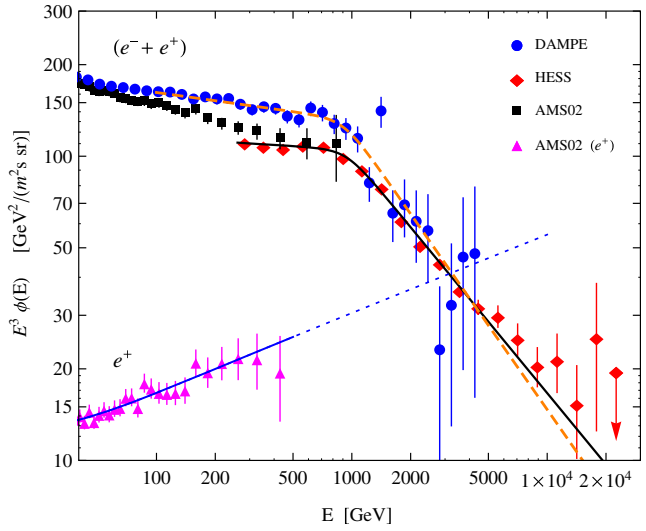


FIG. 5. Measurements of the $(e^- + e^+)$ spectrum obtained by AMS02 [13], DAMPE [18], and HESS, and of the $e^+$ flux by AMS02. The lines are fits of the DAMPE [18] and HESS [21] data.

of Eq. (3), obtaining, for the best-fit parameters, a break energy $E_b \simeq 0.94 \pm 0.02^{+0.29}_{-0.21}$ TeV, spectral indices $\Gamma_1 = 3.04 \pm 0.01^{+0.010}_{-0.18}$ (below the break) and $\Gamma_2 = 3.78 \pm 0.02^{+0.017}_{-0.06}$ (above the break), and a narrow width $w = 0.12 \pm 0.01^{+0.19}_{-0.05}$.

The DAMPE Collaboration fits the data using a form that is a little different from the form of Eq. (3) adopted here, and used by HESS:

$$\phi(E) = K\left(\frac{E}{E_0}\right)^{-\gamma_1}\left[1+\left(\frac{E}{E_b}\right)^{-(\gamma_2-\gamma_1)/s}\right]^s. \quad (6)$$

Equations (3) and (6) are different parametrizations of the same ensemble of curves, but the parameter $s$, used in Eq. (6), and the width $w$ in Eq. (3) are not identical [25] but related by

$$s = w/|\Delta\alpha|. \quad (7)$$

DAMPE finds, for best-fit parameters, a break energy $E_b \simeq 0.914 \pm 0.098$ TeV, $\Gamma_1 = 3.09 \pm 0.01$, $\Gamma_2 = 3.92 \pm 0.20$, with the value of $s$ fixed at 0.1 (which corresponds roughly to $w = 0.083$).

In addition, VERITAS published a fit [23] with a broken power-law form (which is $w \to 0$) where the best-fit break energy $E_{\rm Veritas} \simeq 0.71 \pm 0.04$ TeV is somewhat lower than the estimates of HESS and DAMPE.

The imperfect agreement between the different measurements suggests the existence of some systematic effects, and for this reason, we will not attempt to perform a global fit to all data. Even in the presence of these uncertainties, the existence of a sharp break in the spectrum of the sum $(e^- + e^+)$ should be considered as solidly established.

### B. Observed features in the $e^{\mp}$ spectra

A useful quantity to study the properties of a CR spectrum is the (energy-dependent) spectral index, defined in Eq. (2). Figure 6 shows the spectral indices of the $e^-$, $e^+$ and $(e^- + e^+)$ fluxes calculated from fits to the data. For the AMS02 data we use the best-fit functions presented in this work; for the DAMPE [18] and HESS [21] data we use the fits obtained in the original publications.

The main points that emerge from a study of the measurements of the electron and positron spectra are the following:

(1) For $E \lesssim 20$ GeV the $e^-$ and $e^+$ spectra have a "curved" shape, with spectral indices that change continuously. In this energy range the effects of solar modulations are important, and the estimate of the interstellar spectra is model dependent. In this work we have shown that if the solar modulations are modeled with the FFA approximations, the interstellar spectra for both electrons and positrons are consistent with unbroken power laws. This is an intriguing result that clearly requires a more detailed study.

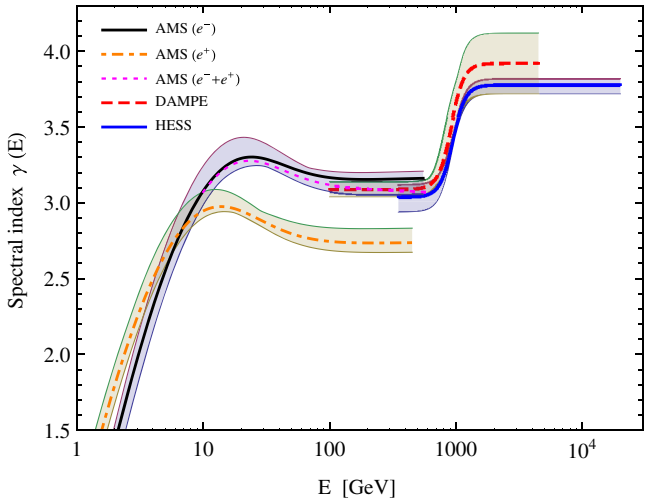


FIG. 6. Spectral indices of the $e^-$, $e^+$ and $(e^- + e^+)$ fluxes. The index is calculated from Eq. (2) using analytic expressions to fit the data. The fits to the AMS02 data are discussed in the text. The fits to the DAMPE and HESS data are from [18] and [21]. The shaded regions are estimates of the $1\sigma$ uncertainties.

(2) The spectral indices for $e^-$ and $e^+$ have a similar behavior in the energy range 10–40 GeV, reaching a maximum at $E \simeq 20$ GeV, and then reaching an approximately constant value (with a step $\Delta\gamma \simeq 0.15$ for electrons and 0.24 for positrons). The existence of this structure was first noted by the AMS02 Collaboration [6]. Both spectra therefore have gradual hardenings at $E \sim 30$ GeV, generated by a mechanism (or mechanisms) that need to be clarified (a more detailed discussion can be found in Appendix).

(3) In the energy range 40–400 GeV both the $e^-$ and $e^+$ spectra can be reasonably well described by simple power laws. Electrons have a significantly softer spectrum ($\gamma_{e^-} \simeq 3.17$, $\gamma_{e^+} \simeq 2.74$). The electron spectrum is much steeper than the proton one.

(4) The spectrum of the sum $(e^- + e^+)$ exhibits a sharp and large break at $E \simeq 1$ TeV. This (together with the "GZK cutoff") is perhaps the most prominent spectral structure is all of the cosmic ray data.

(5) From the published data, it is not possible to reach a firm conclusion about the spectral shape of the separate spectra of $e^-$ and $e^+$ above $E \gtrsim 500$ GeV.

(6) At $E \approx 1$ TeV, the sum $(e^- + e^+)$ is dominated by electrons (extrapolating the lower energy data as unbroken power laws, one estimates a ratio $e^-/e^+ \simeq 3$–4). Therefore, the measurements of the $(e^- + e^+)$ flux imply that the electrons have a spectral break at $E \simeq 1$ TeV. On the other hand, one can also conclude that the positron spectrum cannot continue as an unbroken power law and must undergo a softening at $E \lesssim 1.5$ TeV, because in the absence of such a break, the $e^+$ flux would emerge

as the dominant component of the $(e^- + e^+)$ spectrum, in contrast to the observation (see Fig. 5). The $e^+$ spectral break could develop at the same energy as for electrons, but it could also be at lower (perhaps as low as 600 GeV) or higher energy.

(7) At present, the measurements of DAMPE extend to 4.5 TeV, and those of HESS to 20 TeV, and the data above the break at 1 TeV appear to be consistent with a power-law spectrum. This is in fact a significant constraint for the modeling of the CR sources.

The question we want to investigate is where in the electron and positron spectra it is possible to identify signatures associated with energy losses. To address this question we study some simple models of CR propagation to see what kind of effects one could expect to see.

## III. THEORETICAL MODELS FOR COSMIC RAY SPECTRA

### A. Formation of CR spectra

In general, the flux of cosmic rays of type $j$ and energy $E$ that are observed at the point $\vec{x}$ at time $t_{\rm obs}$ can be written as the convolution:

$$\phi_j(E,\vec{x},t_{\rm obs}) = \frac{\beta c}{4\pi} n_j(E,\vec{x},t_{\rm obs}) = \frac{\beta c}{4\pi}\int_{-\infty}^{t_{\rm obs}} dt_i \int d^3x_i \int dE_i q_j(E_i,\vec{x}_i,t_{\rm obs}-t_i)\mathcal{P}_j(\vec{x},E,\vec{x}_i,E_i,t_{\rm obs}-t_i). \quad (8)$$

In this equation the factor $\beta c/(4\pi)$ relates, assuming isotropy, the flux to the particle density $n_j$. The CR density is obtained as the integral over space, time, and initial energy of an integrand that is the product of two fundamental quantities: the source spectrum $q_j(E_i,\vec{x}_i,t_i)$ and the propagation function $\mathcal{P}_j(\vec{x},E,\vec{x}_i,E_i,t)$. The source spectrum (with dimensions $L^{-3}T^{-1}E^{-1}$) is the rate of particles of type $j$ and energy $E_i$ that are released in interstellar space per unit volume around the point $\vec{x}_i$ at the time $t_i$. The propagation function (with dimensions $L^{-3}E^{-1}$) expresses the probability that a particle of type $j$, created with energy $E_i$ at point $\vec{x}_i$ and $t$ the time $t_i$, is then found at time $t_i + t$ with energy $E$ at point $\vec{x}$.

Equation (8) is a general expression for the CR fluxes, valid for most types of models. The most important nontrivial hypothesis that enters into the equation is the assumption that (with respect to CR propagation) the Galaxy is in a stationary state so that the propagation function $\mathcal{P}_j$ is only a function of the time difference $t = t_{\rm obs} - t_i$.

In most cases Eq. (8) is only a formal solution for the formation of the CR fluxes because it can be very difficult to compute the propagation functions, but in the following we discuss two simple models where the functions $\mathcal{P}_j$ have exact analytic expressions.

Integrating the propagation function over $\vec{x}$ and $E$, one obtains the probability that a particle (created at point $\vec{x}_i$ with energy $E_i$) is still confined in the Galaxy after a time $t$:

$$\int d^3x \int dE \mathcal{P}_j(\vec{x},E,\vec{x}_i,E_i,t) = P_{\rm surv}(E_i,\vec{x}_i,t). \quad (9)$$

This survival probability must be in the interval [0,1], and it decreases monotonically with $t$, with the (physically obvious) limits $P_{\rm surv} = 1$ for $t \to 0$, and $P_{\rm surv} = 0$ for $t \to \infty$.

The average residence time in the Galaxy for a particle created at point $\vec{x}_i$ with energy $E$ is then

$$\langle t_{\rm res}(E,\vec{x}_i)\rangle = \int_0^\infty dt t \left|\frac{dP_{\rm surv}(E,\vec{x}_i,t)}{dt}\right|. \quad (10)$$

### B. Energy losses

The main mechanisms of energy losses for relativistic electrons and positrons traveling in interstellar space are synchrotron radiation and Compton scattering, and the rate of energy loss is reasonably well approximated with the form

$$-\frac{dE}{dt} \equiv \beta(E) \simeq bE^2 \simeq \frac{4}{3}\sigma_{\rm Th} c[\rho_B + \rho_\gamma^*(E)]\frac{E^2}{m_e^2}. \quad (11)$$

In this expression $\sigma_{\rm Th}$ is the Thomson cross section, $\rho_B = B^2/(8\pi)$ is the energy density stored in the magnetic field, and $\rho_\gamma^*(E)$ is the energy density in target photons with energy $\varepsilon \lesssim m_e^2/E$. This kinematical constraint ensures that the $e\gamma$ scatterings are in the Thomson regime, excluding collisions at higher center-of-mass energy (in the Klein-Nishina regime) where the cross section is suppressed.

Other mechanisms, such as bremsstrahlung and ionization, give smaller contributions to the energy loss, and it is a reasonable approximation to neglect them and use the simple expression of Eq. (11) that grows quadratically with energy.

Because of the dependence on $\rho_B$ and $\rho_\gamma$, the rate of energy loss is not constant in space. In this work, however, we make the approximation to consider the Galactic confinement volume as homogeneous, taking for $\rho_B$ and $\rho_\gamma$ a constant average value.

In the vicinity of the Solar System, the magnetic field is of order $B \simeq 3\ \mu$G, with a corresponding energy density $\rho_B \simeq 0.22\ {\rm eV/cm^{-3}}$. The magnetic field is larger near the

Galactic center but also falls rapidly with the distance from the Galactic equatorial plane. The interstellar radiation field is formed by three components: the cosmic microwave background radiation (CMBR), stellar light, and dust emitted infrared radiation. The CMBR homogeneously fills all space with an energy density $\rho_{\rm CMBR} \simeq 0.260$ eV/cm$^3$ formed by very soft photons (with average energy $\langle\varepsilon\rangle \simeq 6.3 \times 10^{-4}$ eV), which are an effective target also for high energy photons. Stellar light and infrared radiation have, in the solar neighborhood, an energy density of order 0.5 eV/cm$^3$, which, however, changes rapidly in space. In the following, when needed, we use as a first-order estimate the value $\langle\rho_B + \rho^*_\gamma\rangle \simeq 0.5$ eV/cm$^3$. One should keep in mind that this average depends on the size and shape of the CR confinement volume, which are very poorly known. It is straightforward to rescale the results for a different estimate if desired.

From the rate of energy loss it is possible to compute a characteristic time for energy loss:

$$T_{\rm loss}(E) = \frac{E}{|dE/dt|} \simeq \frac{1}{bE}. \tag{12}$$

In the last equality we have used the quadratic form for the energy loss $\beta(E) = bE^2$; this results in the dependence $T_{\rm loss} \propto E^{-1}$. A numerical estimate is

$$T_{\rm loss}(E) \simeq 621.6 \left[\frac{0.5\ \text{eV cm}^{-3}}{\langle\rho_B + \rho^*_\gamma\rangle}\right]\left[\frac{\text{GeV}}{E}\right]\ \text{Myr}. \tag{13}$$

If the energy loss is considered as a stationary, continuous process that does not depend on the space coordinates, the energy of a particle is a well-determined function of time. The three quantities $\{E_i, E_f, t\}$ (that is, the initial and final energy of a particle that propagates for a time $t$) are related by the equation

$$\int_{E_f}^{E_i} \frac{dE'}{\beta(E')} = t. \tag{14}$$

This equation can be solved to obtain any one of the three quantities as a function of the other two. For $\beta(E) = bE^2$ one has simple explicit expressions:

$$E_f(E_i, t) = \frac{E_i}{1 + bE_i t}, \tag{15}$$

$$E_i(E_f, t) = \frac{E_f}{1 - bE_f t} \tag{16}$$

[for the assumptions made, one must have $E_f(E, t) = E_i(E, -t)$], and

$$t(E_i, E_f) = \frac{1}{bE_f} - \frac{1}{bE_i}. \tag{17}$$

The limit of $t(E_i, E_f)$ for $E_i \to \infty$ is finite, indicating that electrons and positrons observed at the Earth with energy $E_f$ have a maximum age:

$$t_{\rm max}(E_f) = \lim_{E_i\to\infty} t(E_i, E_f) = \int_{E_f}^{\infty} \frac{dE'}{\beta(E')} \simeq \frac{1}{bE_f}. \tag{18}$$

### C. Leaky box model

The simplest model to describe the Galactic cosmic ray spectra is the so-called leaky box model. In the model the space dependence of the cosmic ray fluxes and sources is neglected, and each CR species is entirely described by the function $n(E, t)$ that gives the density of the particles as a function of energy and time (in the following the subscript $j$ that indicates the particle type will be left implicit). The time evolution of $n(E, t)$ is controlled by the equation

$$\frac{\partial n(E,t)}{\partial t} = q(E,t) - \frac{n(E,t)}{T_{\rm esc}(E)} + \frac{\partial}{\partial E}[\beta(E) n(E,t)]. \tag{19}$$

The spectrum of one particle type is therefore entirely determined by three functions: the source spectrum $q(E, t)$, the escape time $T_{\rm esc}(E)$, and the rate of energy loss $\beta(E)$.

The propagation function (which obviously cannot depend on the space coordinates) is determined by $T_{\rm esc}(E)$ and $\beta(E)$, and has the form

$$\mathcal{P}(E, E_i, t) = P_{\rm surv}(E_i, t)\delta[E - E_f(E_i, t)]. \tag{20}$$

In this expression the delta function expresses the fact that (using the assumption of continuous energy loss) a CR particle has a well-defined energy at all times. The function $P_{\rm surv}(E_i, t)$ is the probability that a CR particle released in interstellar space with energy $E_i$ is still in the Galaxy after a time interval $t$, and can be calculated as

$$P_{\rm surv}(E_i, t) = \exp\left[-\int_0^t \frac{dt'}{T_{\rm esc}[E_f(E_i, t')]}\right]. \tag{21}$$

If energy losses are negligible [that is, in the limit $\beta(E) = 0$], the survival probability becomes a simple exponential $P_{\rm surv}(E, t) = e^{-t/T_{\rm esc}(E)}$. In this case $T_{\rm esc}(E)$ is also exactly equal [see Eq. (10)] to the average residence time of the particles.

The CR density can be calculated using the general expression of Eq. (8). The integration over $E_i$ can be performed using the delta function, obtaining a general solution in the form of one single integral over time:

$$n(E) = \int_0^{t_{\rm max}(E)} dt \frac{\beta[E_i(E,t)]}{\beta(E)} q[E_i(E,t), t] P_{\rm surv}[E_i(E,t), t], \tag{22}$$

where $t_{\rm max}(E)$ is the maximum residence time in the Galaxy for a particle observed with energy $E$

[see Eq. (18)], and $E_i(E,t)$ is the past energy of a particle observed with energy $E$ [see Eq. (16)].

If the source spectrum is constant in time and energy losses are negligible (so that $E = E_i$, with the survival probability, is a simple exponential), the time integration is trivial, and one obtains the simple and obvious result

$$n(E) = q(E)T_{\rm esc}(E). \tag{23}$$

If the CR source is stationary and the escape probability is negligible (that is, in the limit $T_{\rm esc} \to \infty$), the survival probability is unity, and the CR spectrum becomes

$$n(E) = \frac{1}{\beta(E)}\int_E^\infty dE_i q(E_i). \tag{24}$$

A phenomenologically interesting case is as follows:

(i) The source spectrum is stationary in time, confined to the Galactic plane, and constant, with a simple power-law form

$$q(E,\vec{x}) = q_0 E^{-\alpha}\delta[z]. \tag{25}$$

(ii) The escape time is also a power law: $T_{\rm esc}(E) = T_0 E^{-\delta}$.

(iii) The rate of energy loss is quadratic in energy [$\beta(E) = bE^2$], and therefore the loss time is $T_{\rm loss} = 1/(bE)$.

In this situation the critical energy $E^*$ defined by the condition that the escape and loss time are equal is given by

$$E^* = (T_0 b)^{1/(\delta-1)}. \tag{26}$$

The form of the CR spectrum in the limits of low and high energy can be obtained from the more general expressions of Eqs. (23) and (24). These asymptotic solutions are power laws with exponents $(\alpha+\delta)$ at low energy and $\alpha+1$ at high energy:

$$n(E) = \begin{cases} q_0 T_0 E^{-(\alpha+\delta)} & \text{for } E \ll E^* \\ q_0/[b(\alpha-1)]E^{-(\alpha+1)} & \text{for } E \gg E^*. \end{cases} \tag{27}$$

The general solution can be written in the form

$$n(E) = (q_0 T_0)E^{-(\alpha+\delta)}F_{\rm loss}^{\rm LB}(a) \tag{28}$$

which is the product of the no-energy-loss solution multiplied by a correction factor that can be expressed as a function of the energy-dependent parameter $a$:

$$a = \frac{T_{\rm esc}(E)}{T_{\rm loss}(E)} = \left(\frac{E}{E^*}\right)^{1-\delta}. \tag{29}$$

The function $F_{\rm loss}^{\rm LB}(E)$ is given by

$$F_{\rm loss}^{\rm LB}(a) = \int_0^{1/a} d\tau(1-a\tau)^{\alpha-2} \times \exp\left[-\frac{1}{a(1-\delta)}[1-(1-a\tau)^{1-\delta}]\right]. \tag{30}$$

It is straightforward to check that in the limit $a \to 0$, one has $F_{\rm loss}^{\rm LB} \to 1$; while for $a \gg 1$ one has

$$F_{\rm loss}^{\rm LB}(a) \simeq [a(\alpha-1)]^{-1} = (\alpha-1)^{-1}(E/E^*)^{\delta-1}, \tag{31}$$

recovering the asymptotic expressions for $E \ll E^*$ and $E \gg E^*$ in Eq. (27).

Having found an exact expression for the CR spectrum, it is straightforward to compute the energy dependence of the spectral index $\gamma(E)$. The effect of energy losses is to generate a "step" in the index of size ($\Delta\gamma = 1-\delta$), as the spectrum slope changes from the value $(\alpha+\delta)$ at low energy to the values $\gamma = (\alpha+1)$ at high energy. Some examples of the spectral feature generated by energy losses, calculated for the set of assumptions outlined above, are given in Fig. 7.

The step in the spectral index is centered at an energy proportional to $E^*$ [defined in Eq. (26)] but is approximately a factor of 2 smaller. The width of the energy range where the step develops is very broad and depends strongly on $\delta$ (and more weakly also on $\alpha$). For $\delta \simeq 0.5$ the step $\Delta\gamma$ develops when the particle energy grows by a factor of approximately 30, and this corresponds to a width $w$ of order 1.6 to 1.7 (depending on $\alpha$). For $\delta \simeq 0$, the step in spectral index develops when the energy grows by a factor of order 5, and the width $w$ is of order 0.4 to 0.6.

### D. Diffusion model

The idea of describing the propagation of cosmic rays in the Milky Way as diffusion was introduced by Morrison, Olbert, and Rossi in the 1950s [26] and then discussed

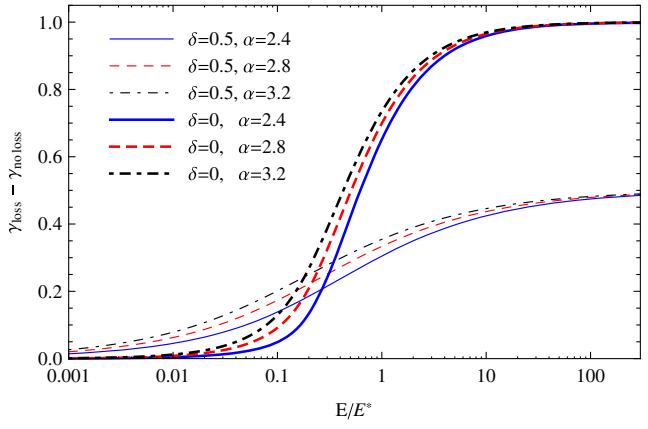


FIG. 7. Spectral feature generated by energy losses calculated in a leaky box model. The source spectrum and the escape time have energy dependence $q(E) \propto E^{-\alpha}$ and $T_{\rm esc}(E) \propto E^{-\delta}$.

extensively by Ginzburg and Syrovatskii [27]. At present, it is the basis for essentially all models for the propagation of CR in the Galaxy.

In this work we use the simplest possible diffusive propagation model, where the CR confinement volume is taken in the (infinitely large) region of space with $|z| \leq H$ (with the $z$ plane coincident with the Galactic equatorial plane). In the confinement volume the effects of the magnetic field are described as isotropic diffusion with a diffusion coefficient $D(E)$ that is a function of rigidity, but it is independent of position [28]. The two surfaces $z = \pm H$ are considered absorption barriers, and particles that reach these surfaces leave the Galaxy permanently. Particles (of a given type) in the diffusive volume lose energy with a space-independent rate described by $\beta(E)$. The model is therefore entirely defined by the "halo size" $H$ and by the two functions $\beta(E)$ and $D(E)$.

Some important quantities in the model are the loss time $T_{\rm loss}(E)$, the diffusion or escape time $T_{\rm diff}(E)$, the critical energy $E^*$, the diffusion radius $R(E_i, E_f, t)$, and the maximum diffusion radius $R_{\rm loss}(E)$.

The loss time has been defined in Eq. (12), and the diffusion time,

$$T_{\rm diff}(E) \equiv T_{\rm esc}(E) = \frac{H^2}{2D(E)}, \tag{32}$$

is the time after which a particle of constant energy $E$, diffusing in a homogeneous medium with diffusion coefficient $D(E)$, travels an average distance $\langle x^2\rangle = \langle y^2\rangle = \langle z^2\rangle = H^2$. It can be demonstrated [29] that this quantity is equal to the average escape time from the Galaxy for a particle of energy $E$ created on the Galactic plane $z = 0$. The critical energy $E^*$ is determined by the condition $T_{\rm loss}(E^*) = T_{\rm esc}(E^*)$.

The quantity $R^2(E_i, E_f, t)$ is equal to the average square distance ($R^2 = \langle x^2\rangle = \langle y^2\rangle = \langle z^2\rangle$) traveled by a particle of initial energy $E_i$ (and final energy $E_f$) propagating in a homogeneous medium with diffusion coefficient $D(E)$ for a time $t$. The propagation includes the effects of energy losses [determined by the function $\beta(E)$], but it neglects absorption effects. The quantity can be calculated by performing one the three integrals:

$$\begin{aligned} R^2(E_i, E_f, t) &= 2\int_0^t dt' D[E_i(E_f, t')] \\ &= 2\int_0^t dt' D[E_f(E_i, t')] = 2\int_{E_f}^{E_i} dE' \frac{D(E')}{\beta(E')}. \end{aligned} \tag{33}$$

The three quantities $E_i$, $E_f$, and $t$ are not independent because they are related by Eq. (14); therefore, $R$ can be expressed as a function of any pair of variables out of the set $\{E_i, E_f, t\}$. In the limit of negligible energy losses, one has $E_i = E_f$ and $R^2(E, t) = 2D(E)t$.

The maximum diffusion radius $R_{\rm loss}(E)$ is the maximum value of $R$ for particles with final (observed) energy $E$, and it corresponds to the limit for $E_i \to \infty$ of $R(E_i, E, t)$. This quantity is finite if the rate of energy loss grows sufficiently rapidly with $E$.

In the following we consider again the phenomenologically interesting case where the rate of energy loss is quadratic in energy [$\beta(E) = bE^2$] and the diffusion coefficient is a power law with exponent $\delta$ ($D(E) = D_0 E^\delta$). In this situation the loss time has the form $T_{\rm loss}(E) = 1/(bE)$, and the diffusion time is also a power law [$T_{\rm esc}(E) = (H^2/(2D_0))E^{-\delta}$]. This implies that the critical energy $E^*$ is

$$E^* = \left(\frac{H^2 b}{2D_0}\right)^{1/(\delta-1)}. \tag{34}$$

The maximum diffusion radius is finite and has the form

$$R^2_{\rm loss}(E) = \frac{2D_0}{b(1-\delta)} E^{-(1-\delta)} = \frac{H^2}{1-\delta}\frac{T_{\rm loss}(E)}{T_{\rm esc}(E)} = \frac{H^2}{1-\delta}\left(\frac{E}{E^*}\right)^{\delta-1}. \tag{35}$$

If (as is expected) $\delta < 1$, the maximum diffusion radius decreases with energy $\propto E^{-(1-\delta)/2}$.

For a finite value of $E_i$ [or for a time $t < t_{\rm max}(E)$], the diffusion radius is

$$\begin{aligned} R^2(E_i, E_f, t) &= R^2_{\rm loss}(E_f)\left[1 - \left(1 - \frac{t}{t_{\rm max}(E)}\right)^{1-\delta}\right] \\ &= R^2_{\rm loss}(E_f)\left[1 - \left(\frac{E_f}{E_i}\right)^{1-\delta}\right]. \end{aligned} \tag{36}$$

In the simple diffusive model that we have just described, the propagation function can be written explicitly:

$$\begin{aligned} \mathcal{P}(\vec{x}, E, \vec{x}_i, E_i, t) = \frac{1}{2\pi R^2} e^{-r^2/(2R^2)} \frac{1}{H} g\left(\frac{z}{H}, \frac{z_i}{H}, \frac{R^2}{H^2}\right) \\ \times \delta[E - E_f(E_i, t)] \end{aligned} \tag{37}$$

where $R$ is the diffusion distance defined above in Eq. (33).

Inspecting Eq. (37) one can see that the propagation along the $x$ and $y$ directions is described by a simple Gaussian, while in the $z$ direction, one has to take into account the presence of the absorption planes at $z = \pm H$, and the propagation has a more complicated expression, encoded in the function $g$.

The solution of the diffusion equation in the presence of the two absorption barriers can be obtained (see e.g., [30]) as the solution without the barriers but including, together with the real source at point $x_i$, an infinity of "mirror"

sources and sinks located symmetrically in the unphysical region outside the region between the two barriers.

Putting the absorption barriers at $\pm 1$, and using adimensional variables for $x$, $x_i$, and $\sigma^2$, the solution takes the form

$$g(x, x_i, \sigma^2) = \frac{1}{\sqrt{2\pi}\sigma} \sum_{n=-\infty}^{+\infty} [e^{-[x-x_n^+(x_i)]^2/(2\sigma^2)} - e^{-[x-x_n^-(x_i)]^2/(2\sigma^2)}]. \tag{38}$$

This expression contains infinite sources located at the points

$$x_n^+ = x_i + 4n \tag{39}$$

(with $x_0^+ = x_i$ the real source) and infinite sinks at the points

$$x_n^- = -x_i + 4n + 2. \tag{40}$$

The solution for the problem where the absorption barriers are at $z = \pm H$ can be obtained simply by rescaling the expression in Eq. (38). Some numerical examples of the function $g(x, x_i, \sigma^2)$ are shown in Fig. 8. The function is always positive in the interval $[-1, 1]$, vanishing at the boundary points ($x = \pm 1$). For $\sigma^2 \ll 1$ the function is, to a good approximation, a simple Gaussian of unit normalization and width $\sigma$ centered at the point $x = x_i$.

A useful property of the function $g$ is that

$$\int_0^\infty d\tau g(x, x_i, \tau) = \begin{cases} (1+x)(1-x_i) & \text{for } x < x_i \\ (1-x)(1+x_i) & \text{for } x > x_i. \end{cases} \tag{41}$$

Having an explicit analytic expression for the propagation function, it is straightforward to compute the CR spectrum for arbitrary forms of the energy-loss function $\beta(E)$ and the diffusion coefficient $D(E)$ and for any source

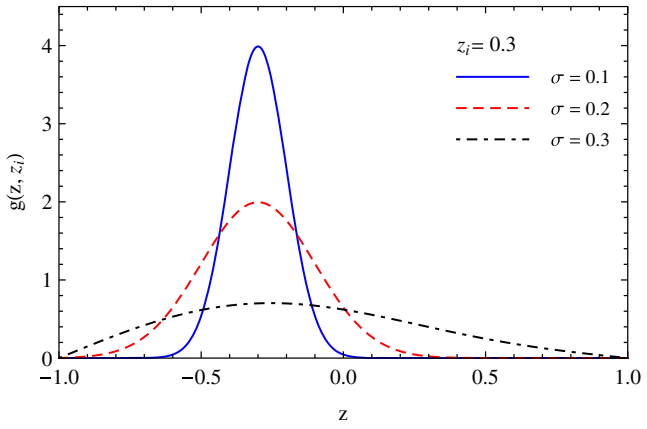


FIG. 8. Examples of the function $g(x, x_i, \sigma^2)$.

spectrum $q(E, \vec{x}, t)$ numerically performing the integrations in Eq. (8).

If one makes the assumptions that

(i) the observation point is on the plane $z = 0$, and
(ii) the source spectrum is constant in time, confined to the plane $z = 0$ and homogeneous in the plane,

then the integration over space and energy in Eq. (8) is trivial, and the CR density can be expressed as an integral over time:

$$n(E) = \frac{1}{H} \int_0^{t_{\max}(E)} dt \frac{\beta[E_i(E,t)]}{\beta(E)} \times q[E_i(E,t), t] g\left(0, 0, \frac{R^2[E_i(E,t), t)}{H^2}\right). \tag{42}$$

The last integration must, in general, be performed numerically; however, in the limit where the energy loss is negligible—that is, for $\beta(E) = 0$ when $E_i = E$, $t_{\max}(E) \to \infty$ and $R^2(E,t) = 2D(E)t$—making use of Eq. (41), the integration can be done analytically, with the result $n(E) = q(E)T_{\rm esc}(E)/H$.

If one makes the additional assumptions that

(iii) the source spectrum is a power law: $q(E) = q_0 E^{-\alpha}$,
(iv) the diffusion coefficient is also a power law: $D(E) = D_0 E^{\delta}$, and
(v) the rate of energy loss is quadratic in energy: $\beta(E) = bE^2$,

then the CR spectrum in the limit of no energy loss takes the power-law form

$$n(E) \simeq n_0(E) = \frac{q(E)T_{\rm esc}(E)}{H} = \frac{q_0 H}{2D_0} E^{-(\alpha+\delta)}. \tag{43}$$

An exact solution can also be found if the escape of the Galaxy can be neglected (this corresponds to the limit $H \to \infty$, or $T_{\rm loss}/T_{\rm esc} \ll 1$). In this limit the function $g$, which describes propagation in the $z$ direction, simply becomes a Gaussian, and the CR density takes the form

$$n(E) \simeq n_{\rm loss}(E) = k(\alpha,\delta) \frac{q(E)T_{\rm loss}(E)}{R_{\rm loss}(E)} = k(\alpha,\delta)\sqrt{1-\delta} \frac{q_0}{\sqrt{2D_0 b}} E^{-(\alpha+(1+\delta)/2)} \tag{44}$$

where $k(\alpha, \delta)$ is an adimensional constant of order unity that depends on the exponents $\alpha$ and $\delta$:

$$k(\alpha,\delta) = \frac{1}{\sqrt{2\pi}} \int_0^1 d\tau' \frac{(1-\tau')^{\alpha-2}}{\sqrt{1-(1-\tau')^{1-\delta}}}. \tag{45}$$

In the general case, the CR spectrum can be written in the form

$$n(E) = n_0(E) F^{\rm diff}_{\rm loss}(a) = \frac{q(E) T_{\rm esc}(E)}{H} F^{\rm diff}_{\rm loss}(a) \qquad (46)$$

as the product of the no-energy-loss expression times a correction factor that depends on the ratio $E/E^*$ via the parameter $a$:

$$a = \left(\frac{E}{E^*}\right)^{1-\delta} = \frac{T_{\rm diff(E)}}{T_{\rm loss}(E)}. \qquad (47)$$

The function $F^{\rm diff}_{\rm loss}(a)$ has the form

$$F^{\rm diff}_{\rm loss}(a) = \int_0^{1/a} d\tau (1 - a\tau)^{\alpha-2} g[0, 0, \sigma^2(a, \tau)] \qquad (48)$$

with

$$\sigma^2(\tau, a) = \frac{1}{(1-\delta)a}[1 - (1 - a\tau)^{1-\delta}]. \qquad (49)$$

It is straightforward to see that in the limit $a \to 0$ one has $F^{\rm diff}_{\rm loss}(0) = 1$, while in the limit $a \to \infty$ one finds $F^{\rm diff}_{\rm loss} \propto a^{-1/2} \propto E^{-(1-\delta)/2}$. The exact expression is

$$\lim_{a\to\infty} F^{\rm diff}_{\rm loss}(a) = k(\alpha, \delta)\sqrt{\frac{1-\delta}{a}}. \qquad (50)$$

These results are consistent with the asymptotic behaviors given in Eqs. (43) and (44). The CR density has spectral index $\alpha + \delta$ at low energy ($E/E^* \ll 1$) and index $\alpha + (1+\delta)/2$ at high energy ($E/E^* \gg 1$).

The transition from low to high energy behavior has a shape that is completely determined by the exponents $\alpha$ and $\delta$. Some examples of this transition are shown in Fig. 9.

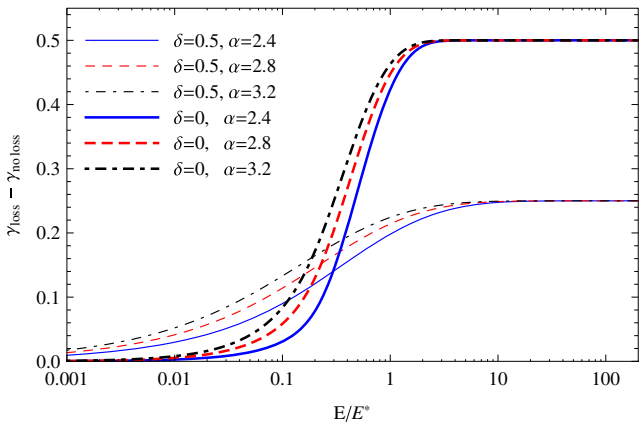


FIG. 9. Spectral feature generated by energy losses in a diffusive model. The diffusion coefficient is homogeneous in the finite layer $|z| < H$ and has the energy dependence $D(E) = D_0 E^\delta$. The CR source is confined in a thin layer at $z \simeq 0$ and has the form $q(E) = q_0; E^{-\alpha}$.

The step in the spectral index is again centered at an energy that is proportional to $E^*$ (but a factor 0.4–0.5 smaller) and develops in a region of $\log E$ of order 1–2 (a factor 3–10). This approximately a factor of 2 smaller than in the case of the leaky box but still a rather gradual break.

Figures 7 and 9 show the shape of the spectral features imprinted on the $e^\mp$ fluxes by the effects of energy loss for two specific (and simple) models that are significantly different from each other. A comparison of these results suggests that the effects of energy losses can generate spectral structures with a detailed shape that depends on the properties of CR propagation in the Galaxy. However, the existence of these (energy loss) softening features appears to be a robust prediction that can be considered model independent. The energy $E^*$ (where the spectral features are centered) can, in general, be interpreted as the point where energy losses become important and therefore measures, with only little model dependence, the average residence time of CR in the Galaxy. The study of the spectral shapes of the $e^\mp$ around $E^*$ can provide additional valuable information for CR Galactic propagation.

It is well known that a diffusion model not only allows us to compute the flux as a function of position but also the dipole $\vec{d}$ of the angular distribution at each point:

$$\phi(E, \Omega, \vec{x}) = \phi(E, \vec{x})[1 + \vec{d}(E, \vec{x}) \cdot \hat{u}(\Omega)] \qquad (51)$$

[where $\hat{u}(\Omega)$ is a versor in the direction $\Omega$]. The dipole momentum is antiparallel to the gradient of the CR density with the value

$$\vec{d}(E, \vec{x}) = -\frac{3D(E)}{\beta c}\frac{\vec{\nabla} n(E, \vec{x})}{n(E, \vec{x})}. \qquad (52)$$

For the simple model we have constructed (with the Solar System exactly on the Galactic plane, and the CR homogeneously distributed on the plane), the dipole at the position of the Sun is zero.

### E. Energy-loss softening feature

In the discussion above we have calculated, in some detail, the shape of the CR spectra for electrons and positrons, assuming a very simple model for the source (which is an unbroken power law) and two simple models of propagation. The main result is that the observable spectrum, which is in fact easy to predict, exhibits a clear "softening feature" with a spectral index that has a "step" around the energy $E^*$. The calculations performed above give a detailed description of the shape of the softening feature [see Eqs. (30) and (48)]. Given the simplicity of these models it is, however, possible (in fact likely) that these detailed predictions are only an imperfect description of the real fluxes. On the other hand, the prediction of the existence of a softening feature (in both $e^-$ and $e^+$ spectra) should be considered a robust prediction, and the identification of these structures is a very

important task. The shape of the softening features (after their identification) could then be used to constrain the modeling of CR propagation in the Galaxy.

## IV. DISCRETE SOURCES

The source of primary Galactic cosmic rays (such as protons and electrons) can very likely be modeled as the emission from an ensemble of discrete astrophysical "events" that can be approximated as pointlike and short-lived for Galactic space and time scales. Accordingly, the flux can be written as the sum of components, in the form

$$\phi(E) = \sum_k \phi_{s,k}(E). \tag{53}$$

In the "standard paradigm" [27,31] the sources of CR protons and electrons are supernovae explosions, but other possibilities (e.g., gamma ray bursts) have been considered. If positrons are generated in interstellar space by a standard mechanism of secondary production, the source is smoothly distributed in space and time; however, the possibility that the main source of $e^+$ is acceleration in astrophysical objects (such as young pulsars) has been the subject of many studies.

Several authors (see e.g., [32]) have discussed the idea that if CR of a certain type $(p, e^-, e^+, \ldots)$ are indeed generated in discrete astrophysical events, the "granularity" of the source could have observable consequences. In this section we discuss this problem and show that the discrete nature of the sources should become manifest for electrons (and also for positrons, if they are generated in discrete accelerators) above a minimum energy (which we will denote $E^\dagger$) that could be as low as a few hundred GeV (depending on the properties of the CR sources and propagation). The effects of the source granularity should be significantly smaller for protons and nuclei and should become observable only at much higher energy.

The fundamental idea in this discussion is simple. It is intuitive that if a large number of source events contribute to the generation of the observed flux of cosmic rays, it is a good approximation to consider the source as continuous; on the contrary, if the CR flux is generated by only a few source events, one can expect observable effects. When the particle energy $E$ increases, the space-time volume where the observed CR particles have their origin shrinks, and therefore the number of source events that contribute to the flux becomes smaller. At sufficiently high energy the effects of the discreteness of the sources (if the sources are indeed discrete) should become manifest.

The discrete nature of the sources can become visible via effects on the angular and energy distribution of the CR flux. An excess (or scarcity) of sources in one direction can clearly generate an anisotropy in the angular distribution of the CR particles, and similarly, an excess (scarcity) of near source events can result in a hardening (softening) of the flux with respect to the smooth behavior predicted for a continuous distribution.

There are two important difficulties in constructing a prediction for the critical energy for source granularity $E^\dagger$. The first one is that the effects that can reveal this granularity are model dependent. The second, more fundamental difficulty is that the observable effects depend on the real distribution in space and time of the sources that generate the cosmic rays, and this distribution is unknown. Different configurations in space and time of the sources closer to the Solar System can result in observational effects that are very different (and of very different sizes).

Keeping these difficulties in mind, we construct some predictions for the energy $E^\dagger$ as a guide to interpret existing and future observations. The predictions are based on three elements: (i) a model for CR propagation in the Galaxy, (ii) a model for the sources, and (iii) a criterion to estimate when the granularity effect should become manifest.

To describe the propagation of CR in the Galaxy, we use the diffusion model presented in Sec. III D. The model (for one particle type) is entirely defined by four parameters that can be chosen as $\{b, H, E^*, \delta\}$, which is the constant that describes energy loss ($|dE/dt| = bE^2$), the vertical size of the CR halo, the critical energy $E^*$, and the exponent that describes the rigidity dependence of the diffusion coefficient.

To keep the discussion as simple as possible, we assume that the source events are all identical, each generating a CR population $Q_0 E^{-\alpha}$. The CR source spectrum can then be written as the sum

$$q(E, \vec{x}, t) = Q_0 E^{-\alpha} \sum_k \delta[\vec{x} - \vec{x}_k]\delta[t - t_k] \tag{54}$$

with the index $k$, which runs over all source events. The quantities $\vec{x}_k$ and $t_k$ are the position and time of the $k$th event. It is obviously not possible to predict the space-time positions of the source events, but one can make assumptions about the probability distribution for these events. We assume that the source events form on the Galactic plane, independently from each other, with a constant probability density (per unit time and unit area) $p_s$:

$$p_s(\vec{x}, t) = \frac{n_s}{T_s}\delta[z]. \tag{55}$$

In this equation the quantity $T_s^{-1}$ is the frequency of source events in the entire Galaxy (so if supernova explosions are the dominant CR source, then $T_s \simeq 50$ years), and $n_s$ is the probability density per unit area for one source event in the disk of the Galaxy, taken in the vicinity of the Solar System.

To estimate $n_s$ one can use studies of the space distributions for possible classes of sources such as supernovae remnants (SNR) [33] or pulsars [34]. These observations show the sources are indeed confined to a narrow

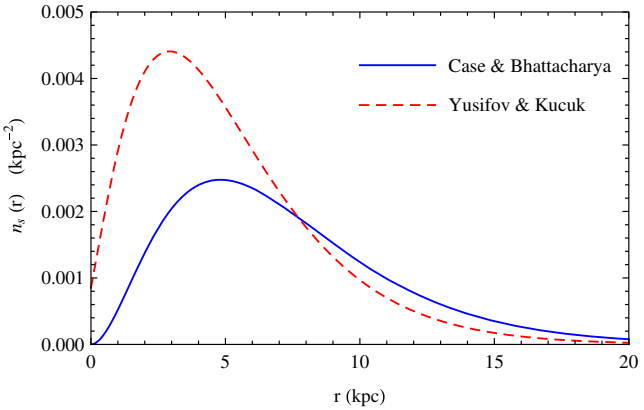


FIG. 10. Fits of the radial distribution of pulsars (Yusifov and Kucuk [34]) and supernova remnants (Case and Bhattacharya [33]) in the Mikly Way ($r$ is the distance from the Galactic center).

layer close to the Galactic equator and have a distribution in the plane that can be fitted with a cylindrically symmetric form $n_s(r)$ (with $r$ the distance from the Galactic center), which (by construction) satisfies the normalization condition

$$\int d^2 r n_s(r) = 1. \tag{56}$$

The fits obtained in [33,34] are shown in Fig. 10. The detailed form of $n_s(r)$ can be used as a template for numerical studies of cosmic ray production. In this work, however, we simply take $n_s$ as a constant: $n_s = n_s(r_\odot) \simeq 0.0015$ kpc$^{-2}$, with the value at the position of the Solar System. This is a reasonable approximation because at high energy only sources not too distant from the Earth give significant contributions to the CR flux (see discussion below), and $n_s(r)$ changes rather slowly with $r$. The (average properties) of the source model are then determined by four parameters: $\{n_s, T_s, Q_0, \alpha\}$.

Combining the propagation and source models, the description of the CR flux for one particle type depends on a total of 8 parameters: $\{b, E^*, H, \delta\}$ for propagation and $\{n_s, T_s, Q_0, \alpha\}$ for the source model. In the discussion below we consider two parameters ($b$ and $n_s$) as fixed. The parameter $b$ (which describes the rate of energy loss) has a value $b \simeq 0$ for $p$ and $\bar{p}$, while for $e^\mp$ one has $b \simeq 5.10 \times 10^{-17}$ (GeV s)$^{-1}$ [see Eq. (13)]. The value of $n_s$ (the surface density of the source events normalized to unity in the entire Galaxy) has been discussed above (see Fig. 10) and, in a reasonably good approximation, is determined by the size of the Galactic disk: $n_s \approx (\pi R_{\rm disk}^2)^{-1}$. The two other parameters ($\alpha$ and $Q_0$) can be determined by the condition that the calculation matches the observed spectrum (in spectral shape and absolute normalization). This leaves four parameters as free: $\{T_s, H, E^*, \delta\}$.

Smoothing out the discreteness of the events, the CR source takes the stationary form:

$$\langle q(E, \vec{x}) \rangle = \frac{n_s}{T_s} Q_0 E^{-\alpha} \delta[z]. \tag{57}$$

This source spectrum (with the identification $q_0 = Q_0 n_s / T_s$) is in fact identical to the source spectrum of Eq. (25) discussed in Sec. III D. The question that we are addressing here is under which conditions one can expect observable differences between the flux generated by the smoothed-out source spectrum of Eq. (57) and the flux generated by an ensemble of discrete sources as in Eq. (54).

All models where the combination $Q_0 n_s / T_s$ has the same value have the same smoothed-out source spectrum; however, this spectrum can be generated by an ensemble of frequent and faint events (small $T_s$ and small $Q_0$) or an ensemble of rare and bright events (large $T_s$ and large $Q_0$). It is obvious that in the second case the source granularity is easier to observe.

The simple criterion that we use to estimate the conditions for which the granularity of the sources is manifest is the condition that one single source generates a large fraction of the flux. It is clearly desirable to express this qualitative idea in a more precise form. For this purpose one can introduce the concept of the cumulative flux $\phi_{\rm cum}(N_s, E)$, which is the sum of the largest $N_s$ contributions to the total flux at energy $E$.

Having a model for the sources and for CR propagation, the cumulative flux can be calculated for a smoothed-out distribution of the source spectrum to determine the conditions for which the brightest source event accounts for one-half of the observed flux. It is intuitive (and it will also be demonstrated in detail below) that for a fixed model of sources and propagation, the fraction of the total flux associated with the brightest source grows with energy; one can therefore solve for $E$:

$$\frac{\phi_{\rm cum}(1, E)}{\phi(E)} = \frac{1}{2} \tag{58}$$

to calculate an energy $E^\dagger$ that we interpret as a best estimate of where the source granularity effects should become manifest.

It should be noted that the criterion that we have constructed for the observability of the source granularity could very well be too stringent, and it is possible that evidence for the existence of discrete sources will be obtained in situations where dozens (and not just one or very very few) sources give significant contributions to the CR flux.

In the following we outline a calculation of the cumulative flux $\phi_{\rm cum}(N_s, E)$.

### A. Flux components

The flux received by one source event at position $\vec{x}$ and time $t$ can be calculated by having a model for the spectrum

of particles generated in the event and a model for CR propagation in the Galaxy. In general, one has

$$\phi_s(E,\vec{x},t) = \int dE_i Q_s(E_i)\mathcal{P}(E,\vec{x}_\odot,E_i,\vec{x},t). \quad (59)$$

In the following we make the (good) approximation that the Solar System is on the Galactic plane; we assume that all source events are on this plane and generate identical spectra of particles with a power-law spectrum $Q_0E^{-\alpha}$. It is then straightforward to find that if energy losses are negligible (that is, for $b \simeq 0$), as is the case for protons and nuclei, the flux from a source event at a distance $r = |\vec{x}_s - \vec{x}_\odot|$ and at time $t$ in the past is

$$\phi_s(E,r,t) = \frac{c}{4\pi}\frac{Q_0E^{-\alpha}}{H^3}\mathcal{G}_0\left(\frac{r}{H},\frac{t}{T_{\rm esc}(E)}\right), \quad (60)$$

where the function $\mathcal{G}_0(\rho,\tau)$ has the form

$$\mathcal{G}_0(\rho,\tau) = \frac{1}{2\pi\tau}e^{-\rho^2/(2\tau)}g(0,0,\tau) \quad (61)$$

[with $g$ defined in Eq. (38)]. The function $\mathcal{G}_0$ satisfies the normalization condition

$$(2\pi)\int_0^\infty d\rho\rho\int_0^\infty d\tau\mathcal{G}_0(\rho,\tau) = 1. \quad (62)$$

In the case where energy losses are the dominant effect for propagation (that is, the case for high energy electrons and positrons, when $E \gg E^*$), the spectrum from a single source is

$$\phi_s(E,r,t) = \frac{c}{4\pi}\frac{Q_0E^{-\alpha}}{R^3_{\rm loss}(E)}\mathcal{G}_{\rm loss}\left(\frac{r}{R_{\rm loss}(E)},\frac{t}{T_{\rm loss}(E)}\right), \quad (63)$$

where the function $\mathcal{G}_{\rm loss}(\rho',\tau')$ has the form

$$\mathcal{G}_{\rm loss}(\rho',\tau') = \frac{1}{(2\pi)^{3/2}\chi^3(\tau')}(1-\tau')^{\alpha-2}e^{-(\rho')^2/[2\chi^2(\tau')]} \quad (64)$$

with

$$\chi^2(\tau') = 1-(1-\tau')^{1-\delta} \quad (65)$$

[note that $\rho' = r/R_{\rm loss}(E)$ can take values in the interval $(0,\infty)$ while $\tau'$ is defined in the interval (0,1)].

The function $\mathcal{G}_{\rm loss}(\rho',\tau')$ satisfies the normalization condition

$$(2\pi)\int_0^1 d\tau'\int_0^\infty d\rho'\rho'\mathcal{G}_{\rm loss}(\rho',\tau') = k(\alpha,\delta) \quad (66)$$

with $k(\alpha,\delta)$ the adimensional quantity given in Eq. (45).

It is important to note that in both cases the shape of the CR flux generated by a source that is observable at the Earth is *not* a simple power law, even if the source spectrum is a power law. This is because particles of different energy (or rigidity) propagate in different ways. This results in an observable spectrum that evolves with time in normalization and in shape.

For both cases considered the flux generated by a single source event at distance $r$ and time $t$ has the scaling form

$$\phi_s(r,t) = \phi^*\mathcal{G}\left(\frac{r}{R},\frac{t}{T}\right) \quad (67)$$

(where the energy dependence has been left implicit). In the case of negligible energy loss, one has $R = H$ and $T = T_{\rm esc}(E)$, while when escape is negligible, one has $R = R_{\rm loss}(E)$ and $t = T_{\rm loss}(E)$. In Eq. (67) $\phi^*$ is a characteristic flux given by

$$\phi^* = \frac{c}{4\pi}\frac{Q_s(E)}{R^3} \quad (68)$$

with $Q_s(E)$ the emission from the source.

Lines of constant value for the contributions of a source event (for some values of the ratio $\phi_s/\phi^*$) in the plane $\{\rho,\tau\}$ are shown in Fig. 11 for the case of negligible energy loss and in Fig. 13 for the case of dominant energy loss.

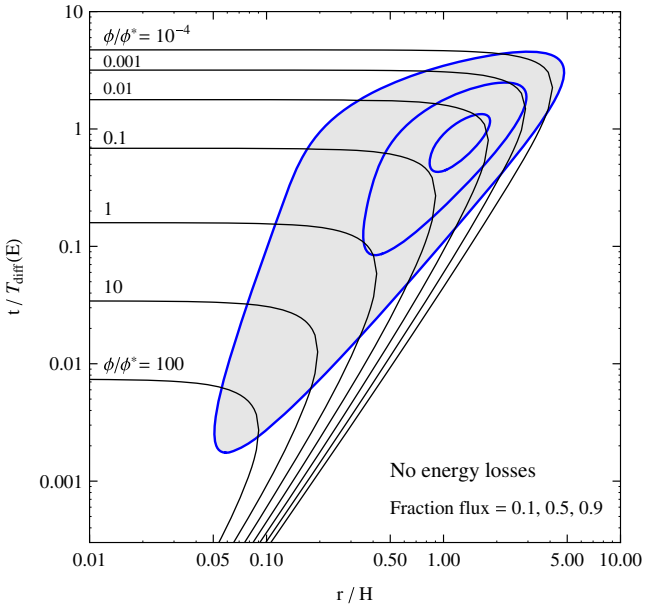


FIG. 11. Space-time distribution of the CR flux (energy losses are considered negligible). The thick closed lines in and around the shaded area are defined by the equation $d\phi/(d\ln r d\ln t) =$ const and chosen so that the integral in the region inside the line corresponds to a fraction 0.1, 0.5, and 0.9 of the total flux. The thinner lines are defined by the equation $\phi_s(r,t)/\phi^* = f$, with $f = 10^{-4}$, $10^{-3}$, $10^{-2}$, $10^{-1}$, 1, 10, and $10^2$.

The contributions from sources at a fixed distance $r$ depend on the time $t$. For a(n) (arbitrary) fixed value of $E$, the flux received from one source initially grows with time, reaching its maximum value at the time $t \simeq r^2/[2D(E)]$, and then decreases slowly. A contribution of a certain size $\phi_s$ can therefore be obtained from events that have a distance $r < r_{\max}(\phi_s)$. For each $r < r_{\max}$ there are two solutions for the age that give the same contribution $\phi_s$. The two solutions correspond to the cases where the flux from the sources is growing or decreasing with time.

A simple but very important point is that, for the model of diffusive propagation that we are discussing here, the contribution to the flux of each source event has an associated dipole momentum in the direction of the source, whose size can be calculated using the general expression of Eq. (52).

The vanishing dipole momentum of the total flux for the smoothed-out source spectrum is the effect of the cancellation of the dipoles of the different source events that are located symmetrically around the Solar System, but the contribution of the closest source events will not balance exactly because of stochastic effects. If few sources contribute to the flux, one can expect large anisotropic effects.

### B. Space-time distribution of the CR source

It is instructive to study the size and shape of the space-time volume where the cosmic rays observed at the Earth are generated. In general, the space-time distribution of the CR sources can be calculated from the knowledge of the source spectrum and the propagation function as

$$\frac{d\phi(E,\vec{x}_i,t)}{d^3x_i dt} = \int dE_i q(E_i,\vec{x}_i,t)\mathcal{P}(E,\vec{x}_\odot,E_i,\vec{x}_i,t) \qquad (69)$$

(where $t=0$ is the present, and $\vec{x}_\odot$ is the position of the Solar System).

For the model we are discussing here, and a smoothed-out source spectrum, the space-time volume takes a simple scaling form in the cases of negligible energy loss and negligible escape probability. In the first case one finds

$$\left.\frac{d\phi(E,r_i,t)}{d^2r dt}\right|_{\text{no losses}} = \frac{\phi(E)}{H^2 T_{\text{esc}}(E)}\mathcal{G}_0\left(\frac{r}{H},\frac{t}{T_{\text{esc}}(E)}\right) \qquad (70)$$

where $r$ is the distance of the source event, and the function $\mathcal{G}_0(\rho,\tau)$ is given in Eq. (60). A graphic representation of the function $\rho^2\tau\mathcal{G}_0(\rho,\tau)$ [which is proportional to the distribution $d\phi/(d\ln r d\ln t)$] is shown in the form of a contour plot in Fig. 11. The $\rho$ and $\tau$ distributions of the source can be obtained by integrating over the other variable, and they are shown in Fig. 12.

These results show that CRs observed at the Earth have their origin in a time interval of order $T_{\text{esc}}(E)$ (with the contributions of older emission suppressed exponentially) and in a space region that is approximately a disk centered on the position of the Solar System with a radius of order $H$ (and again the contributions of more distant sources are suppressed exponentially).

The time interval in which the observed CRs are produced becomes shorter with increasing energy because $T_{\text{esc}}(E)$ decreases $\propto E^{-\delta}$; on the other hand, the space region where the CRs are produced is energy independent. This is the result of a cancellation: Particles of higher energy have a shorter Galactic residence time but also a larger diffuse coefficient; the result is a propagation distance that is independent from energy.

For the case in which energy losses are the dominant effect in propagation, the space-time distribution of the source takes the form

$$\left.\frac{d\phi(E,r,t)}{d^2r dt}\right|_{\text{no escape}} = \frac{\phi(E)}{R^2_{\text{loss}}(E)T_{\text{loss}}(E)}\frac{1}{k(\alpha,\delta)} \times \mathcal{G}_{\text{loss}}\left(\frac{r}{R_{\text{loss}}(E)},\frac{t}{T_{\text{loss}}(E)}\right) \qquad (71)$$

where the function $\mathcal{G}_{\text{loss}}(\rho',\tau')$ is given in Eq. (64).

The function $(\rho')^2\tau'\mathcal{G}_{\text{loss}}(\rho',\tau')$ is shown in the form of a contour plot in Fig. 13, and the $\rho'$ and $\tau'$ distributions (obtained by integrating over the other variable) are shown in Fig. 14.

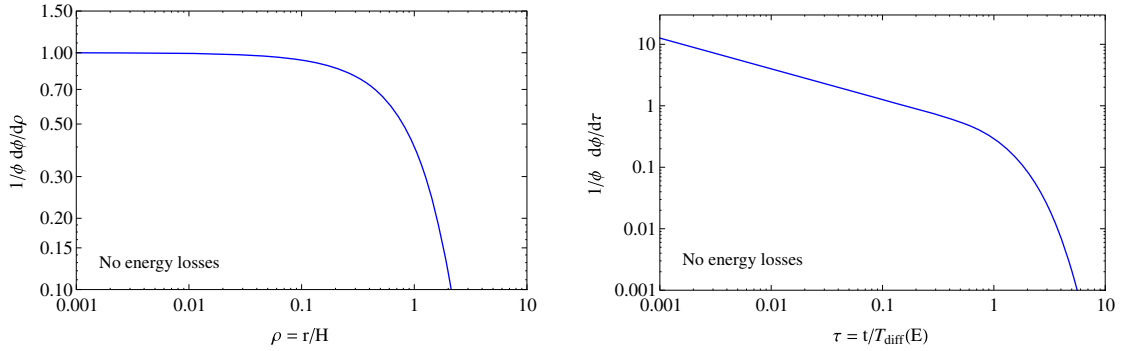


FIG. 12. Space and time distribution of the CR sources (energy losses are considered to be negligible). Left panel: Plot of $1/\phi d\phi/d\rho$ versus $\rho = r/H$. Right panel: Plot of $1/\phi d\phi/d\tau$ versus $\tau = t/T_{\text{esc}}(E)$.

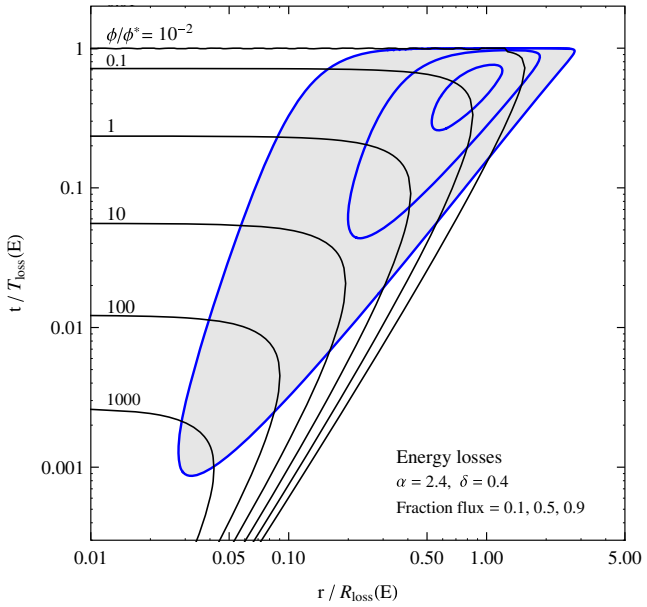


FIG. 13. Space-time distribution of the CR flux (energy losses are considered to be dominant). See Fig. 11 for the meaning of the different lines. The calculation is performed by assuming that the source spectrum is a power law with exponent $\alpha = 2.4$, and the diffusion coefficient has the energy dependence $D_0 E^\delta$ with $\delta = 0.4$.

These results demonstrate that, in this case, CRs observed at the Earth have their origin in a time interval of order $T_{\rm loss}(E)$ and in a space region that is approximately a disk of radius $R_{\rm loss}(E)$, with the contributions of older and more distant sources suppressed exponentially.

The time $T_{\rm loss}$ decreases with energy $\propto E^{-1}$, and the radius $R_{\rm loss}(E)$ decreases $\propto E^{-(1-\delta)/2}$ (because the growth with $E$ of the diffusion coefficient is not sufficiently rapid to compensate for the shorter propagation time). The space-time volume of the CR sources therefore shrinks rapidly with energy $\propto E^{-(2-\delta)}$, much more rapidly than in the case where the energy loss is negligible.

### C. Cumulative flux

Assuming that the CR flux is formed by the sum of the contributions of discrete events and considering a smoothed-out source (so that the quantities $N_s$ and $\phi_s$, which are the number of sources and the size of source contribution, can be considered as continuous variables), it is straightforward to compute the differential distributions $dN_s/d\phi_s$, which give the number of sources with flux in the interval $[\phi_s, \phi_s + d\phi_s]$, and $d\phi/d\phi_s$, which gives the flux generated by contributions in the same size interval. For the model discussed here, these quantities can be calculated by performing the integrals

$$\frac{dN_s}{d\phi_s} = \frac{n_s}{T_s}\int d^2r \int dt \delta[\phi_s - \phi_s(r,t)], \tag{72}$$

$$\frac{d\phi}{d\phi_s} = \frac{n_s}{T_s}\int d^2r \int dt \phi_s \delta[\phi_s - \phi_s(r,t)] \tag{73}$$

(where we have left the energy dependence implicit). Using the results of Sec. IV A and the general form of the flux from each source of Eq. (67), one finds that the distributions have the simple scaling forms

$$\frac{dN_s}{dx} = N^* \mathcal{A}(x), \tag{74}$$

$$\frac{d\phi}{dx} = N^* \phi^* \mathcal{B}(x) \tag{75}$$

where $x = \phi_s/\phi^*$, with $\phi^*$ the characteristic flux given in Eq. (68). The energy-dependent quantity $N^*$ is given by

$$N^* = \frac{n_s}{T_s} R^2 T, \tag{76}$$

and in first approximation, it gives the total number of sources that contribute to the CR flux.

The total flux can be expressed in terms of $\phi^*$ and $N^*$ as

$$\phi(E) = kN^*(E)\phi^*(E) \tag{77}$$

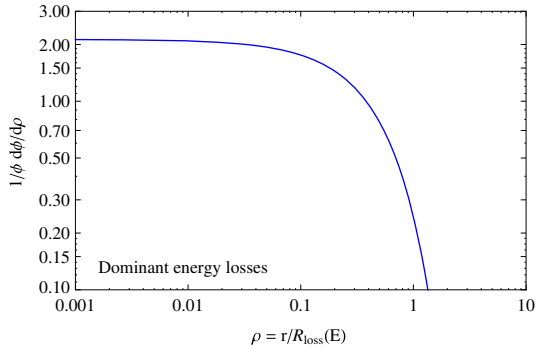


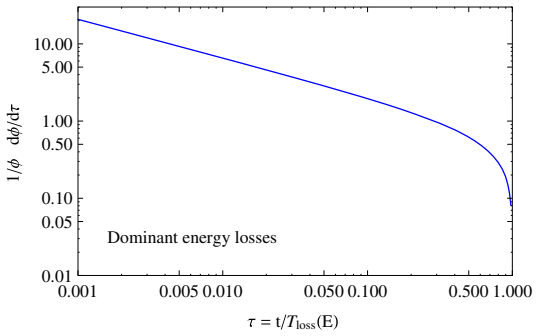


FIG. 14. Space and time distribution of the CR sources (energy losses are dominant). Left panel: Plot of $1/\phi d\phi/d\rho'$ versus $\rho' = r/T_{\rm max}(E)$. Right panel: Plot of $1/\phi d\phi/d\tau'$ versus $\tau' = t/T_{\rm loss}(E)$.

where $k$ is an energy-independent constant given by the integral

$$k = (2\pi)\int_0^{\tau_{\max}}\int_0^{\infty} d\rho\rho\mathcal{G}(\rho,\tau). \tag{78}$$

The quantity $\tau_{\max}$ is the maximum value of $\tau$, and it has the value $\tau_{\max}\to\infty$ in the case of negligible energy loss and $\tau_{\max}=1$ when energy loss is dominant in propagation. As shown above, the constant $k$ is unity in the case of negligible energy loss, and for the case where energy losses are dominant, it is given by Eq. (45). The functions $\mathcal{A}(x)$ and $\mathcal{B}(x)$ can be calculated as

$$\mathcal{A}(x) = (2\pi)\int d\rho\rho\int_0^{\tau_{\max}} d\tau\delta[x-\mathcal{G}(\rho,\tau)] \tag{79}$$

$$\mathcal{B}(x) = (2\pi)\int d\rho\rho\int_0^{\tau_{\max}} d\tau x\delta[x-\mathcal{G}(\rho,\tau)]. \tag{80}$$

In the case of negligible energy loss, the functions $\mathcal{A}_0(x)$ and $\mathcal{B}_0(x)$ (which determine the shape of the distributions $dN_s/d\phi_s$ and $d\phi/d\phi_s$) have a universal shape that is independent from the values of the parameters in the model. The functions are shown in Fig. 15. By inspecting the figure one can see that the observed flux is formed by components that have very broad distributions of relative size, which span approximately 6 orders of magnitude.

In the case where energy loss is dominant, the shape of the functions $\mathcal{A}_{\rm loss}(x)$ and $\mathcal{B}_{\rm loss}(x)$ is determined by the values of the exponents $\alpha$ and $\delta$. Two examples are shown in Fig. 16. The two curves (in both panels) are calculated for the combinations $(\alpha=2.4,\ \delta=0.4)$ and $(\alpha=2.6,\ \delta=0)$. Note that in both cases the observed flux (for a smoothed-out source spectrum) has the same spectral index: $\gamma\simeq\alpha+(1+\delta)/2\simeq 3.1$. Also in this case one can see that the CR flux is formed by components that have very different sizes.

It is interesting to discuss how the quantity $N^*(E)$, defined in Eq. (76), depends on the parameters of the model. In the case of negligible energy loss, which is applicable to protons, one has

$$N_p^* = \frac{n_s}{T_s}H^2T_{\rm esc}(E) = \frac{n_s}{T_s}\frac{H^2}{b}(E^*)^{-(1-\delta)}E^{-\delta} \tag{81}$$

(in the second equality the escape time has been expressed as a function of the critical energy $E^*$). The number of sources that generate the flux of protons (and other primary nuclei) decreases with energy $\propto E^{-\delta}$ and has a value that depends on the model parameters as $N_p^*\propto T_s^{-1}H^2(E^*)^{-(1-\delta)}$. The quantity is proportional to the frequency of source events ($T_s^{-1}$), and it becomes smaller when $E^*$ increases (that is, when the CR residence time becomes smaller). A numerical example (for $\delta=1/3$) is

$$N_p^*(E)\simeq 2240\left[\frac{T_s}{50\ {\rm yr}}\right]^{-1}\left[\frac{H}{5\ {\rm kpc}}\right]^{2}\left[\frac{E^*}{3\ {\rm GeV}}\right]^{-2/3}\left(\frac{E}{\rm PeV}\right)^{-1/3} \tag{82}$$

(note that $E$ is measured in PeV). One can see that (for the propagation model considered here) if supernova explosions are the main CR source, the number of events that contribute to the proton flux also remains rather large for energies well above the "knee" (at $E\simeq 3$ PeV). This statement also remains true if the critical energy $E^*$ has a value close to 1 TeV [in this case the estimate in Eq. (82) is reduced to approximately 50].

For the case where energy losses are the dominant effect in propagation, which is relevant for $e^{\mp}$ at high energy, one has

$$N_e^* = \frac{n_s}{T_s}R_{\rm loss}^2(E)T_{\rm loss}(E) = \frac{n_s}{T_s}\frac{H^2}{b(1-\delta)}(E^*)^{(1-\delta)}E^{-(2-\delta)} \tag{83}$$

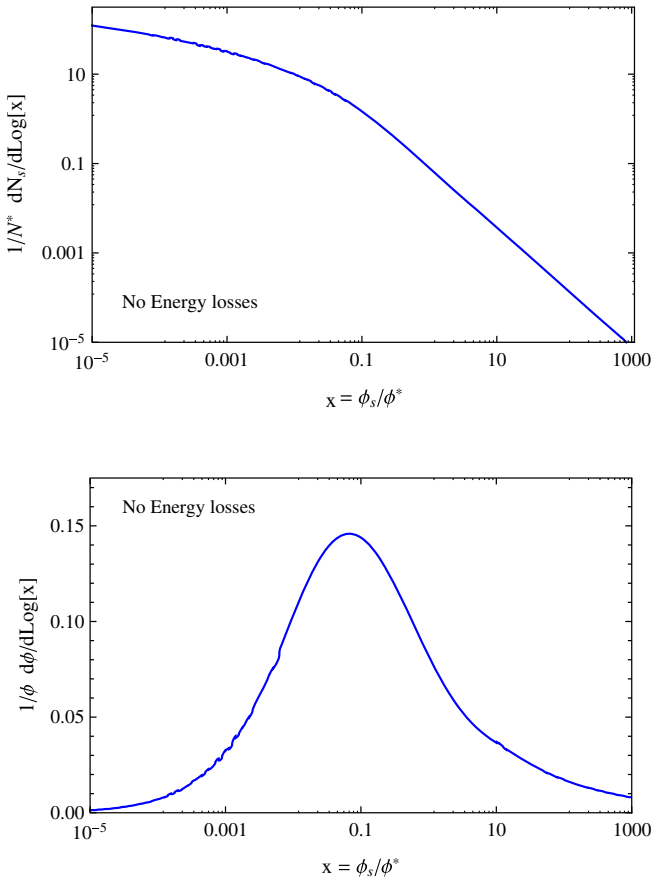


FIG. 15. The top (bottom) panel shows the shape of the distribution $dN_s/d\phi_s$ ($d\phi/d\phi_s$) as a function of $\phi_s$, calculated assuming that energy losses are negligible. The distributions are shown in the energy-independent scaling form, plotting the quantity $1/N^*dN_s/d\ln x$ ($1/\phi d\phi/d\ln x$ in the bottom panel) where $x=\phi_s/\phi^*$ and the quantities $N^*$ and $\phi^*$ are given in Eqs. (76) and (68), with $R=H$ and $T=T_{\rm esc}(E)$.

(again, in the second equality we have expressed $N_e^*$ in terms of the critical energy $E^*$). In this case, the number of sources that contribute to the flux decreases rapidly with energy ($\propto E^{-(2-\delta)}$), reflecting the fact that both $R_{\rm loss}$ and $T_{\rm loss}$ decrease with $E$. The dependence of $N_e^*$ on the parameters of the model is $N_e^* \propto T_s^{-1} H^2 (E^*)^{(1-\delta)}$. Note that in this case the estimate of $N_e^*$ increases with $E^*$. This reflects the fact that with increasing $E^*$ the CR residence time becomes shorter, but the propagation radius grows; this second effect is dominant. A numerical example (for $\delta = 1/3$) is

$$N_e^*(E) \simeq 9.6 \left[\frac{T_s}{50\ \text{yr}}\right]^{-1} \left[\frac{H}{5\ \text{kpc}}\right]^{2} \left[\frac{E^*}{3\ \text{GeV}}\right]^{2/3} \left(\frac{E}{\text{TeV}}\right)^{-5/3} \tag{84}$$

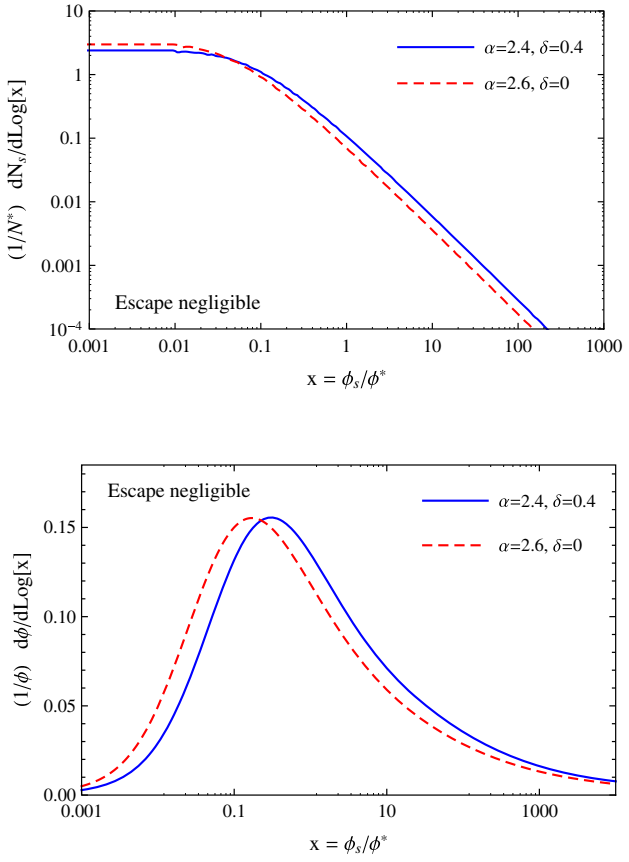


FIG. 16. The top (bottom) panel shows the shape of the distribution $dN_s/d\phi_s$ ($d\phi/d\phi_s$) as a function of $\phi_s$ calculated by assuming that energy losses are dominant for CR propagation (escape is negligible). The distributions are shown in the energy-independent scaling form, plotting the quantity $1/N^* dN_s/d\ln x$ ($1/\phi d\phi/d\ln x$ in the bottom panel) where $x = \phi_s/\phi^*$ and the quantities $N^*$ and $\phi^*$ are given in Eqs. (76) and (68) with $R = R_{\rm loss}(E)$ and $T = T_{\rm loss}(E)$. The shape of the distributions depends on the exponents $\alpha$ and $\delta$, and the curves describe the cases $\{\alpha = 2.6, \delta = 0.4\}$ and $\{\alpha = 2.6, \delta = 0.0\}$.

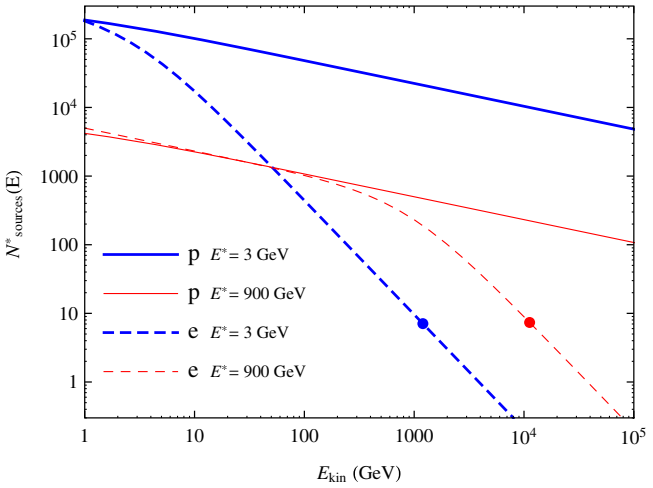


FIG. 17. The curves show, as a function of the kinetic energy $E_k$, the quantities $N_p^*$ and $N_e^*$, which give the (approximate) number of sources that contribute to the observed flux. The curves are calculated using a generalization of Eqs. (82) and (84), assuming that the frequency of sources in the entire Milky Way is $(50\ \text{years})^{-1}$ with $\delta = 0.4$, and for two different values of the critical energy $E^*$: $E^* = 3$ GeV and $E^* = 900$ GeV. The two points along the curves for $N_e^*$ indicate the energy $E_e^\dagger$ [see Eq. (93)] where one expects that granularity effects become dominant.

(note that $E$ is measured in TeV). This estimate shows that if supernova explosions are the sources of electrons, and if the critical energy $E^*$ is in the GeV range (and the CR propagation model used here is reasonably correct), then only a few sources contribute to the flux for $E \gtrsim 1$ TeV.

Figure 17 shows some examples of the energy dependence of $N_p^*(E)$ and $N_e^*(E)$. The curves are calculated by assuming that the frequency of the source events is equal to the estimated rate of supernovae explosions in the Galaxy ($T_s = 50$ yr) and for $\delta = 0.4$. The quantities $N_e^*(E)$ and $N_p^*(E)$ are calculated for two values of the critical energy $E^*$ ($E^* = 3$ GeV and $E^* = 900$ GeV). For $E \ll E^*$, when energy losses are negligible, $N_e^*$ and $N_p^*$ are equal at the same rigidity and (for ultrarelativistic particles) decrease $\propto E^{-\delta}$. For $E \gg E^*$ the number of sources for the electron fluxes rapidly $N_e^* \propto E^{-(2-\delta)}$. It is important to note that $N_p * (E)$ and $N_e^*$ in the energy range $E \lesssim E^*$ are smaller for large $E^*$ because a large $E^*$ corresponds to a shorter residence time of CR in the Galaxy [$T_{\rm esc} \propto (E^*)^{-1}$] and therefore a smaller number of sources that can contribute to the flux. On the other hand, when $E \gg E^*$, the quantity $N_e(E)$ becomes larger when $E^*$ grows because a larger $E^*$ corresponds to faster propagation for the CR particles, and sources from a larger Galactic volume can reach the Solar System, overcompensating the effect of the shorter time integration. The important implication is that for larger $E^*$ the discreteness of the CR sources should become significant at higher energy (see discussion below).

The calculation of $N^*_{e,p}$ already allows a first-order estimate of when the source granularity effects should become visible, using, e.g., the equation $N^*_{e,p}(E^\dagger) \simeq 1$ to calculate the energy where the effects should be large. In fact (as discussed in the following) this simple argument yields results that are, to a good approximation, correct for protons and overestimate the energy $E^\dagger$ by a factor of 3–5 for $e^\mp$. It is, however, desirable to construct a more robust argument for the estimate of $E^\dagger$, as discussed below.

The results of Eqs. (74) and (75) for the differential distributions $dN_s/d\phi_s$ and $d\phi/d\phi_s$ imply that the quantities $N_s(\phi_{s,\min})$ [the number of sources that generate a flux larger than $\phi_{s,\min}$] and $\phi_{\rm cum}(\phi_{s,\min})$ [the flux formed by components that have flux larger than $\phi_{s,\min}$] also have a scaling form

$$N_s(\phi_{s,\min}) = N^* \mathcal{A}_{\rm int}\left(\frac{\phi_{s,\min}}{\phi^*}\right) \tag{85}$$

and

$$\phi_{\rm cum}(\phi_{s,\min}) = \phi \mathcal{B}_{\rm int}\left(\frac{\phi_{s,\min}}{\phi^*}\right) \tag{86}$$

where the functions $\mathcal{A}_{\rm int}(x)$ and $\mathcal{B}_{\rm int}(x)$ are given by

$$\mathcal{A}_{\rm int}(x) = \int_x^\infty dx' \mathcal{A}(x'), \tag{87}$$

$$\mathcal{B}_{\rm int}(x) = \frac{1}{k}\int_x^\infty dx' \mathcal{B}(x') \tag{88}$$

[with $k$ given by Eq. (78)]. Combining the last two equations, it is straightforward to express the cumulative flux $\phi_{\rm cum}$ as a function of the $N_s$ (the number of largest sources):

$$\phi_{\rm cum}(N_s) = \phi \mathcal{C}\left(\frac{N_s}{N^*}\right) \tag{89}$$

where the function $\mathcal{C}(m)$ is

$$\mathcal{C} = \mathcal{B}_{\rm int}[\mathcal{A}^{-1}_{\rm int}(m)]. \tag{90}$$

The relation between $\phi_{\rm cum}$ and $N_s$ is shown for the cases of negligible energy loss and negligible escape in Figs. 18 and 19. As already discussed, the shape of the relation between the ratios $\phi_{\rm cum}(N_s)/\phi$ and $N_s/N^*$ is universal (that is, independent from the values of the parameters of the model) for the case of negligible energy losses and depends on the exponents $\alpha$ and $\delta$ when energy losses are dominant.

Having in hand an explicit expression for the cumulative flux as a function of the number of sources [see Eq. (89)], the estimate of the energy where the source granularity

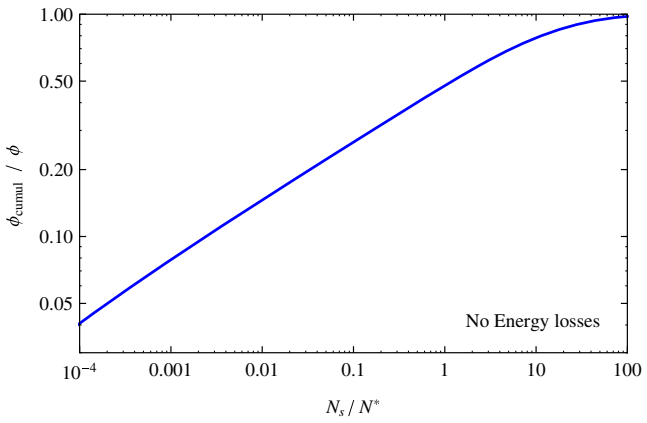


FIG. 18. Cumulative flux $\phi_{\rm cum}$ as a function of the number of source events $N_s$ calculated by assuming that energy losses are negligible. The relation is shown in the energy-independent form $\phi_{\rm cum}(N_s)/\phi$ versus $N_s/N^*$ where $N^*$ is given in Eq. (76) with $R = H$ and $T = T_{\rm esc}(E)$.

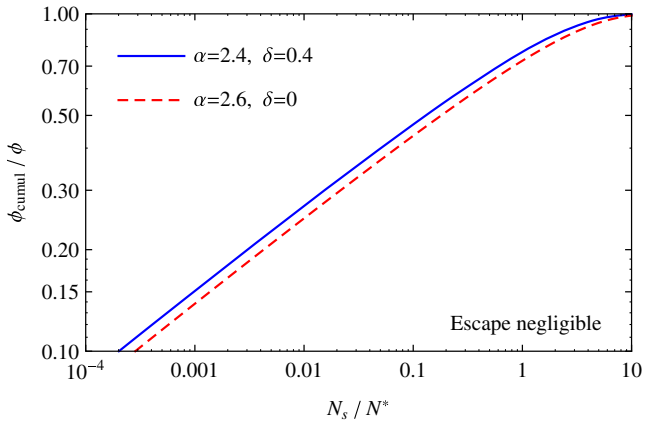


FIG. 19. As in Fig. 18, but with the flux calculated by assuming that energy losses are the dominant effect in propagation. The quantities $N^*$ are defined in Eq. (76) with $R = R_{\rm loss}(E)$ and $T = T_{\rm loss}(E)$. The shape of the curve depends on the exponents $\alpha$ and $\delta$. The two lines in the figure describe the cases $\{\alpha = 2.6, \delta = 0.4\}$ and $\{\alpha = 2.6, \delta = 0.0\}$.

effects should become manifest according to the criterion of Eq. (58) can be stated as

$$N^*(E) = \frac{n_s}{T_s} R^2(E) T(E) \simeq \frac{1}{\mathcal{C}^{-1}(1/2)}. \tag{91}$$

It should be noted that this equation has the same structure as the "naive" criterion $N^*(E) = 1$ [simply replacing unity with the number $\mathcal{C}^{-1}(1/2)$], but it is now derived in a more rigorous way.

Using the calculations of the functions $\mathcal{C}_0(m)$ and $\mathcal{C}_{\rm loss}(m)$ shown in Figs. 18 and 19 [which give $1/\mathcal{C}_0^{-1}(1/2) = 1.23$ and $1/\mathcal{C}_{\rm loss}^{-1}(1/2) = 7.76$ (5.54)

for the choice of parameters $\{\alpha = 2.6, \delta = 0.4\}$ ($\{\alpha = 2.6, \delta = 0.0\}$)], one can obtain quantitative estimates for $E^\dagger$.

In the case of protons (negligible energy losses) the granularity energy has a very high value. For $\delta = 1/3$ one finds

$$(E^\dagger)_p \simeq 5.4 \times 10^{19}\ \text{eV} \left[\frac{T_s}{50\ \text{yr}}\right]^{-35} \left[\frac{H}{5\ \text{kpc}}\right]^{6} \left[\frac{E^*}{\text{TeV}}\right]^{-2} \quad (92)$$

(where we have taken as a "standard reference" the frequency of supernovae in the Milky Way, and a high value for the critical energy $E^*$). Observational evidence for the discreteness of CR protons will therefore very likely be possible only via the observations of subtle, small effects.

For the case of large energy losses, relevant for $e^\mp$, the critical energy $E^\dagger$ is many orders of magnitude smaller. For example, for $\delta = 0.4$ (and therefore $\alpha = 2.4$) one finds

$$(E^\dagger)_{e^\mp} \simeq 1.57\ \text{TeV} \left[\frac{T_s}{50\ \text{yr}}\right]^{-0.625} \left[\frac{H}{5\ \text{kpc}}\right]^{1.25} \left[\frac{E^*}{3\ \text{GeV}}\right]^{0.375}. \quad (93)$$

For $\delta = 0$ (that is, rigidity-independent diffusion), one has

$$(E^\dagger)_{e^\mp} \simeq 0.490\ \text{TeV} \left[\frac{T_s}{50\ \text{yr}}\right]^{-0.5} \left[\frac{H}{5\ \text{kpc}}\right]^{1.0} \left[\frac{E^*}{3\ \text{GeV}}\right]^{0.5}. \quad (94)$$

In Fig. 17 the granularity energy $E_e^\dagger$ is shown for two examples where the critical energy $E^*$ is 3 or 900 GeV (in both cases $T_s = 50$ yr and $\delta = 0.4$). The important point illustrated in this figure is that when $E^*$ is low (and the propagation of the CR particles is slow), the effects of the granularity of the sources become important at lower energy.

If the frequency of the source events that generate the electrons is comparable to SN explosions, and the critical energy is $E^* \lesssim 3$ GeV, then the source granularity effects should be visible at $E$ of order of 1 TeV or less. On the other hand, if $E^* \approx 900$ GeV, of order 1 TeV, then the CRs propagate faster, more sources contribute to the flux, and the granularity effects become visible at an energy approximately 1 order of magnitude higher.

At the moment, there is no clear evidence for effects associated with the discreteness of the sources up to an energy of order 10 TeV. To reconcile the absence of source discreteness effects with the assumption of a low value for the critical energy $E^*$, the frequency of source events must be much higher than a few per century. An alternative solution is to assume a higher value of the critical energy.

## V. INTERPRETATION

In this work we have argued that two crucial problems for the interpretation of the electron and positron cosmic rays are the identification of the effects of energy losses and that of the discreteness of the sources in the observed spectra. After reviewing the existing observations in Sec. II and theoretical models in Secs. III and IV, it is now possible to summarize the main results.

### A. Critical energy $E^*$

On the basis of very general considerations, one can predict that the spectra of both electrons and positrons should exhibit a softening feature at approximately the same energy $E^*$. At this energy the residence time and energy-loss time are approximately equal, and the effects of energy loss become significant. The shape and structure of these softening features should be considered model dependent, but the existence of the features is a robust prediction.

Since the loss time $T_{\text{loss}}(E)$ is determined by well-known physics (with the main uncertainty associated with the shape and size of the CR confinement volume), the identification of $E^*$ corresponds to a measurement of the CR residence time at the energy $E^*$.

The phenomenological study of the $e^\mp$ spectra shows the existence of one clear softening, observed for the sum $(e^- + e^+)$, at $E \approx 1$ TeV. At lower energy (where separate measurements of $e^-$ and $e^+$ spectra are available) it is not easy to identify spectral features that can be interpreted as the signature of energy-loss effects. A possibility, however, is to place $E^*$ below 10 GeV, in the energy range where the exponents of both spectra change continuously, and where solar modulations are important.

One can therefore conclude that there are two alternative possibilities for the value of the critical energy $E^*$. The first one is to have $E^* \lesssim 3$ GeV, well inside the region where solar modulations are important. The second one is to identify the spectral break observed in the $(e^- + e^+)$ spectrum as the energy-loss feature, so that $E^* \simeq 1$ TeV.

The two solutions differ by a very large factor and therefore imply CR residence times that are very different. A critical energy of order $E^* \simeq 3$ GeV implies (for CR of the same rigidity) a residence time of order 200 Myr. Such a long time is in tension (if not in open conflict) with estimates of the CR residence time based on measurements of the abundances of beryllium isotopes [35].

A critical energy of order $E^* \simeq 1$ TeV implies a residence time of order 0.5 Myr. The extrapolation at lower energy depends on the exponent $\delta$ of the escape time [since $T_{\text{esc}}(E) = T_{\text{loss}}(E^*)(E/E^*)^{-\delta}$]. For a rigidity of 10 GV one obtains a residence time of order 1–4 Myr for $\delta = 0.1$–$0.4$. This short residence time is not inconsistent with the beryllium isotope measurements, but it is in conflict with the grammage estimated from the measurements of

secondary nuclei (lithium, beryllium, and boron), assuming that this grammage is accumulated during propagation in interstellar space [36,37].

To establish the validity of the low energy solution for $E^*$, one needs a good understanding of the $e^{\mp}$ interstellar spectra. These spectra are not directly observable and must be inferred from the measured ones by correcting for the effects of solar modulations. This procedure is, at the moment, model dependent. In Sec. II we have shown that if the solar modulations are described with the force field approximation, the interstellar spectra of both $e^-$ and $e^+$ can be well represented as unbroken power-law spectra in the energy range 1–10 GeV. This result is inconsistent with the presence of a softening feature in the same energy range and therefore is in conflict with the hypothesis of a low value for the critical energy. More detailed studies of the solar modulation effects could, in the future, demonstrate that the interstellar $e^-$ and $e^+$ spectra deviate from a simple smooth form the 1–10 GeV range, and that the reconstructed spectral features can be understood as the consequence of energy losses. Alternatively, these studies could yield smooth interstellar spectra and therefore exclude the possibility that $E^*$ is at low energy.

The existence of the spectral break at $E \approx 1$ TeV is clear; however, its shape appears to be narrower than what is predicted by the models we have discussed in this work. If this spectral structure is in fact generated by energy-loss effects, this could require improved models for propagation. It is, however, also clear that it is very desirable to obtain more precise measurements of the spectral shape in this energy range.

It should also be added that if energy losses are not the explanation for the spectral break at 1 TeV, one needs an alternative explanation for its origin, and the apparent narrowness of the observed spectral break is a problem also for these models.

### B. Source granularity

A second, robust prediction for the spectra of electrons is that if the particles are generated in rare events such as supernova explosions or GRB's, the granularity of the source should become visible at sufficiently high energy, when the number of source events that contribute to the observed flux becomes small. The observable effects should be anisotropies for the angular distributions and deviations from a power-law shape for the energy spectra. At very large $E$, when the maximum propagation distance becomes shorter than the distance of the closest source active in a time interval of order $T_{\rm loss}(E)$, the CR flux should become exponentially suppressed.

At the moment, there are only upper limits [38] on the anisotropy of the electron and positron spectra, and the measurements above the spectral break at $E \simeq 1$ TeV of DAMPE, HESS and the other Cherenkov telescopes are consistent with a simple power law up to an energy of order 10–20 TeV.

These results are in tension with the hypothesis that the sources of the electrons are supernova (SN) explosions (that have a known frequency and space density), if the "SN paradigm" is combined with the assumption that cosmic rays have a long Galactic residence time (and the critical energy $E^*$ is of order a few GeV), because in this case [see Eqs. (93) and (94)] one expects large effects already at $E \simeq 500$ GeV.

One explanation for this problem is that the sources that generate the electrons are not SN explosions and have a higher frequency in the Galaxy. An alternative possibility is to conclude that the propagation distance for CR electrons (and positrons) is longer (and correspondingly the critical energy $E^*$ is higher) so that more objects can contribute to the flux.

## VI. ASTROPHYSICAL IMPLICATIONS

The identification of the critical energy $E^*$ where energy losses become important for CR propagation in the Galaxy has profound implications for cosmic ray astrophysics. In this section we show that $E^*$ can only have values in two distinct energy intervals, that is, $E^* \lesssim 3$ GeV ("low critical energy hypothesis") or $E^* \gtrsim 900$ GeV ("high critical energy hypothesis"). In this second case, it is natural to identify $E^*$ with the energy where the $(e^- + e^+)$ spectrum has a break, and therefore $E^* \approx 900$ GeV. These two solutions for the critical energy have important and very different implications.

If $E^*$ is at high energy, then we have the following conditions.

(i) The electron and proton source spectra must have different shapes. This is an important constraint on the structure and properties of the CR accelerators.

(ii) The positron and antiproton spectra can be well described under the hypothesis that the main source for both types of antiparticles is the standard mechanism of secondary production.

(iii) Cosmic rays propagate over long distances, and therefore more distant sources can contribute to the flux. In the multi-TeV energy range the number of sources that generate the $e^-$ flux can then be sufficiently large so that source granularity effects remain small and the spectrum smooth.

(iv) The spectral break in the $(e^- + e^+)$ at $E \approx 1$ TeV can be naturally interpreted as the signature of energy-loss effects.

(v) The residence time of a CR particle with a rigidity of order $\approx$1 GV is predicted to be of order $\approx$1 Myr. This can be directly tested in a model-independent way with measurements of the isotope abundances in the beryllium flux.

(vi) The interpretation of the fluxes of secondary nuclei (such as lithium, beryllium, and boron) likely

requires that most of the nuclei are generated by fragmentation of primary nuclei inside (or in the envelope) of the CR accelerators.

If $E^*$ is at low energy, then we have the following conditions:

(i) The difference in spectral shape between the electron and proton (in the energy interval 10–900 GeV) can be attributed to energy-loss effects imprinted on source spectra of equal shape.
(ii) A new hard source of positrons (in addition to the standard mechanism of secondary production) is required.
(iii) The propagation distance that $e^{\mp}$ of TeV energy can travel is short, and therefore only or few accelerator sources can contribute to the flux. This has to be reconciled with the observed spectral shape of the all-electron flux.
(iv) The spectral break in the all-electron flux must be attributed to properties of the sources.
(v) The residence time of CR particles with rigidity ≈1 GV is predicted to be of order ≈300 Myr.
(vi) The measurements of the fluxes of secondary nuclei (Li, Be, and B) are consistent with the hypothesis that they are mostly formed in interstellar space.

To understand the origin of the CR spectra, it is very instructive to compare the spectra of $p$, $e^-$, $\bar{p}$, and $e^+$. The four energy distributions are shown in Fig. 20. In the energy interval 30–400 GeV, the spectra of $e^{\mp}$ and $\bar{p}$ can be well described as simple power laws:

$$\phi_j(E) \simeq K_j \left(\frac{E}{E_0}\right)^{-\gamma_j} \tag{95}$$

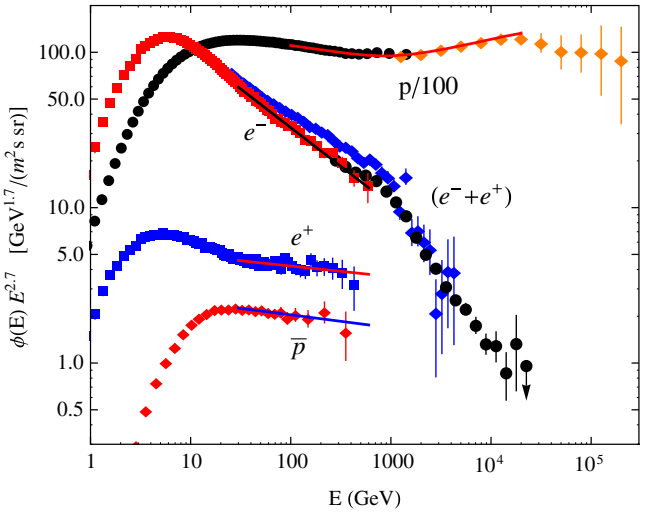


FIG. 20. Spectra of $p$, $e^-$, $e^+$, $(e^- + e^+)$, and $\bar{p}$. The high energy data points for protons are from CREAM [39]; the data points for $(e^- + e^+)$ are from DAMPE and HESS. All other points are from AMS02. The lines superimposed to the $e^-$, $e^+$, and $\bar{p}$ data points are simple power-law fits for $E > 30$ GeV. The line for the proton data is a broken power-law fit taken from [9].

TABLE IV. Power-law fits to the CR spectra.

| Particle | $K$ (m$^2$ s sr)$^{-1}$ | $\gamma$ | $N_{\text{d.o.f.}}$ | $\chi^2_{\text{min}}$ |
|---|---|---|---|---|
| $e^-$ | $(1.19 \pm 0.01) \times 10^{-3}$ | $3.20 \pm 0.01$ | 30 | 12.7 |
| $e^+$ | $(1.14 \pm 0.02) \times 10^{-4}$ | $2.77 \pm 0.02$ | 29 | 12.0 |
| $\bar{p}$ | $(5.6 \pm 0.2) \times 10^{-5}$ | $2.78 \pm 0.03$ | 12 | 1.6 |
| $p$ (low $E$) | $(0.301 \pm 0.002)$ | $2.790 \pm 0.005$ | 12 | 1.6 |
| $p$ (high $E$) | $(0.210 \pm 0.001)$ | $2.61 \pm 0.01$ | 9 | 19.7 |

(with $E_0$ an arbitrary energy scale that we will fix at the value $E_0 = 50$ GeV). The results of fits based on Eq. (95) are listed in Table IV.

In the case of protons, an unbroken power law cannot describe the spectrum because of the existence of a hardening around $E \simeq 300$ GeV. The expression of Eq. (95) can, however, describe the $p$ spectrum in separate energy intervals. For $E \lesssim 300$ GeV the spectral index is of order $\gamma_p^{\text{low}} \simeq 2.80$, while at high energy it is of order $\gamma_p^{\text{high}} \simeq 2.61$. This high energy result is determined by the measurements of CREAM [39].

The comparison of the spectral shapes of the different particle types shows some intriguing results:

(a) The shapes of the $e^-$ and $p$ spectra are very different from each other, and the energy distribution of electrons is much softer. In the energy range 30–400 GeV $\gamma_p \simeq 2.80$, while $\gamma_{e^-} \simeq 3.20$.
(b) The spectral indices of the $e^+$ and $\bar{p}$ fluxes are consistent with being equal to each other with the value $\gamma_{e^+} \simeq \gamma_{\bar{p}} \simeq 2.78$. The positron/antiproton ratio is approximately constant in the energy interval considered with the value $e^+/\bar{p} \approx 2.02$.

The observation that the CR flux (for a certain particle type) has a power-law form in the energy interval $[E_{\text{min}}, E_{\text{max}}]$ suggests that both the source spectrum and the escape time $T_{\text{esc}}(E)$ are of power-law form in the same interval. In the cases of electrons and positrons this also implies (as already discussed) that the critical energy is outside the energy interval considered, that is, either below $E_{\text{min}}$ ("low critical energy hypothesis") or above $E_{\text{max}}$ ("high critical energy hypothesis").

If the standard mechanism of secondary production is the dominant source of CR positrons and antiprotons, the source spectrum for $E \gtrsim 10$ GeV (when threshold and mass effects are negligible) is in fact, to a reasonably good approximation, of power-law form, with an exponent equal to the spectral index of the proton flux:

$$q_{\bar{p}(e^+)}(E,\vec{x}) \simeq 4\pi\sigma_{pp}\Sigma_{\text{ism}}C_{\text{nuclei}}Z_{pp\to\bar{p}(e^+)}(\gamma_p)K_p\left(\frac{E}{E_0}\right)^{-\gamma_p}\delta[z]. \tag{96}$$

Writing this equation we have used the fact that interstellar gas is concentrated in the Galactic disk, $\sigma_{pp}$ is the inelastic

cross section for $pp$ interactions, $\Sigma_{\rm ism}$ is the density per unit area of gas calculated by integrating the density along the $z$ axis, $C_{\rm nuclei} \simeq 1.7$ is an adimensional factor that takes into account the contribution of other CR and target nuclei to the production of antiparticles, and $Z_{pp\to j}(\gamma)$ is the so-called "$Z$ factor," that is, the $(\gamma-1)$ moment of the inclusive spectrum for the production of particle $j$ in $pp$ collisions:

$$Z_{pp\to j}(\gamma) = \int_0^1 dx x^{\gamma-1} \frac{dn_{pp\to j}(x)}{dx}. \tag{97}$$

Secondary particles of energy $E$ are generated by the collisions of protons in a broad energy range $E_p \simeq$ 10–100 $E$, and therefore, in the expression above, one should use the parameters $K_p$ and $\gamma_p$ of protons at higher energy.

A very important point is that the source spectra of antiprotons and positrons are proportional to each other, with an energy-independent ratio:

$$\frac{q_{e^+}(E)}{q_{\bar p}(E)} \simeq \frac{Z_{pp\to e^+}(\gamma_p)}{Z_{pp\to \bar p}(\gamma_p)} \simeq 1.9 \pm 0.3. \tag{98}$$

The numerical estimate of this ratio (and its uncertainty) is determined by modeling of the properties of hadronic interactions (see discussion in the Appendix of [40]).

The observable CR fluxes can be obtained from the source spectra using the results presented in Sec. III D. If energy losses are negligible one has

$$\phi_j(E) = \frac{c}{4\pi} q_j(E) \frac{T_{\rm esc}(E)}{H} = \frac{c}{4\pi} \frac{q_{0,j} T_{\rm esc}(E_0)}{H} \left(\frac{E}{E_0}\right)^{-(\alpha_j+\delta)}, \tag{99}$$

where $\alpha_j$ is the exponent of the source spectrum for particle type $j$, and $\delta$ is the exponent that controls the rigidity dependence of the diffusion time for all particles.

If energy losses are the main effect in the propagation, then the CR flux is

$$\phi_j(E) = \frac{c}{4\pi} \frac{q_{0,j} T_{\rm esc}(E_0)}{H} k(\alpha_j,\delta)\sqrt{1-\delta} \left(\frac{E^*}{E_0}\right)^{\frac{(1-\delta)}{2}} \left(\frac{E}{E_0}\right)^{\alpha_j+\frac{(1+\delta)}{2}} \tag{100}$$

with $k(\alpha,\delta)$ the constant of Eq. (45).

The important point of this discussion is that the spectral index $\gamma_j$ of the CR flux for particle $j$ is determined by the spectral index $\alpha_j$ of the source spectrum and by the exponent $\delta$ of the diffusion time; however, the result depends on whether energy losses are negligible or not. In the first case one has

$$\gamma_j = \alpha_j + \delta, \tag{101}$$

and in the second one,

$$\gamma_j = \alpha_j + \frac{(1+\delta)}{2}. \tag{102}$$

It is therefore clear that scenarios where the critical energy is small ($E^* < E_{\rm min}$) or large ($E^* > E_{\rm max}$) have profoundly different implications.

### A. High critical energy hypothesis

If the critical energy $E^*$ is large (above the maximum energy of the energy interval we are considering), then the propagation properties of protons and electrons are approximately equal. The observation that the spectral indices of $p$ and $e^-$ are different immediately implies that the two particles must have source spectra of different shape, and using Eq. (101) one can deduce that $\alpha_{e^-} - \alpha_p \simeq \gamma_{e^-} - \gamma_p$. Such a conclusion would obviously have important implications for the properties of the CR accelerators.

On the other hand, the assumption that positrons and antiprotons (in the energy interval considered) propagate in approximately the same way is consistent with the hypothesis that the antiparticle fluxes are generated by the standard mechanism. This consistency is quite striking because it emerges from two independent observations. The first one is that the spectral indices are equal within errors:

$$\gamma_{\bar p} \simeq \gamma_{e^+}. \tag{103}$$

The second one is that the ratio $e^+/\bar p$ is (within systematic uncertainties) equal to the ratio for the source spectra:

$$\frac{e^+}{\bar p} \equiv \frac{\phi_{e^+}(E)}{\phi_{\bar p}(E)} \simeq \frac{q_{e^+}(E)}{q_{\bar p}(E)} \simeq \frac{Z_{pp\to e^+}(\gamma_p)}{Z_{pp\to \bar p}(\gamma_p)} \approx 1.9 \pm 0.3. \tag{104}$$

Accepting the result that the antiparticle fluxes are generated by the standard mechanism (and therefore that $\alpha_{e^+} \simeq \alpha_{\bar p} \simeq \gamma_p$), it becomes possible to estimate the value of $\delta$ from Eq. (101) (the exponent that controls the rigidity dependence of the diffusion) and also the spectral index of the proton source $\alpha + p$:

$$\delta \simeq \gamma_{\bar p} - \gamma_p \simeq \gamma_{e^+} - \gamma_p \approx 0.2 \tag{105}$$

and

$$\alpha_p \simeq \gamma_p - \delta \approx 2.4 \tag{106}$$

(where we have used for $\gamma_p$ the result of the fit of the proton flux at high energy). Combining Eqs. (99) and (96) it is also possible to estimate the quantity $T_{\rm esc}(E_0)/H \sim 1$ Myr/Kpc.

### B. Low critical energy hypothesis

If the critical energy $E^*$ is smaller than $E_{\rm min}$, the relation between the observed flux and the source spectrum is different for $p$ and $\bar{p}$ compared to $e^-$ and $e^+$. This offers the interesting possibility to assume that the difference in shape for the fluxes of electrons and protons is generated by propagation. Assuming $\alpha_p \simeq \alpha_{e^-}$, one can use Eq. (100) to estimate $\delta$ and Eq. (99) to estimate $\alpha_p$, with the results

$$\delta = 1 - 2(\gamma_{e^-} - \gamma_p) \simeq 0.2 \tag{107}$$

and (for $E \leq 300$ GeV)

$$\alpha_p \simeq \gamma_p - \delta \simeq 2.6. \tag{108}$$

Using Eq. (100) one can then estimate the ratio of the electron and proton source spectra:

$$\frac{q_{0,e}}{q_{0,p}} = \frac{K_e}{K_p}\left(\frac{E^*}{E_0}\right)^{(\delta-1)/2}\frac{1}{k(\alpha,\delta)} \simeq 0.020\left(\frac{E^*}{3\ \text{GeV}}\right)^{-0.4}. \tag{109}$$

The assumption that the propagation of $e^+$ and $\bar{p}$ is different (because of energy-loss effects for positrons) is, however, in clear conflict with the hypothesis that the main source of antiparticles is secondary production. This conflict is manifest in the observation that the spectral indices of the positron and antiproton fluxes are approximately equal. The relation between the flux and the source spectral indices is now given by Eq. (101) for antiprotons and by Eq. (102) for positrons, so in this case the observation that $\gamma_{e^+} \simeq \gamma_{\bar{p}}$ implies that the shapes of the source spectra are different and

$$\alpha_{\bar{p}} - \alpha_{e^+} \simeq \frac{1-\delta}{2}. \tag{110}$$

This result is in conflict with the hypothesis that antiprotons and positrons are generated by the secondary production mechanism, or also by other mechanisms (such as most models for dark matter self-annihilation or decay) where the $e^+$ and $\bar{p}$ are generated with spectra of similar shape.

The bottom line is that the assumption that the critical energy $E^*$ is below 10 GeV requires the existence of a new source of high energy positrons. The two observations [see Eqs. (103) and (104)] that the spectral indices of the antiproton and positron fluxes are approximately equal, and that the ratio $e^+/\bar{p}$ of the fluxes is of order unity (and equal to the ratio of the hadronic $Z$ factors), are now simply meaningless numerical "coincidences" that constrain the shape and absolute normalization of the new positron source.

The conclusion that the positron flux contains a hard, nonstandard component generates the crucial prediction that the spectrum should exhibit a hardening feature associated with the transition from the regime where the standard mechanism of secondary production is the dominant mechanism of positron production to the regime where the new source is dominant. A discussion of the possible identification of this hardening feature in the positron flux is contained in the Appendix.

## VII. OUTLOOK

The spectra of Galactic cosmic rays observable at the Earth carry very important information about their sources and about the structure of the magnetic field in our Galaxy. The nuclear component (protons and nuclei) dominates the flux, but the study of the smaller electron and positron components is of great importance to understand the mechanisms that shape the spectra. In some sense, the fluxes of $e^-$ and $e^+$ carry more information than the fluxes of protons and nuclei because their spectral shape should show the imprints of energy losses.

In this work we have argued that the effects of energy loss should be significant only above a critical energy $E^*$ and very quickly become dominant for propagation. The spectra of both $e^-$ and $e^+$ should therefore exhibit softening features at approximately the same energy that mark the onset of the regime in propagation where energy losses are important. The identification of the critical energy is a crucial problem for CR astrophysics.

The study of the spectral shapes of the electron and positron spectra suggests for $E^*$ two possible solutions that differ by a large factor and have profoundly different implications.

The first solution, which is in fact implicitly the "orthodody" most commonly (but not universally) accepted, is that the critical energy has a value of order of a few GeV. This implies a very long residence time for CR in the Galaxy, and a nonstandard hard source for positrons in the Galaxy. This "low critical energy" scenario is consistent with the hypothesis that the CR accelerators are released in interstellar space spectra of $e^-$ and $p$, which, in a broad energy range, have the same shape. In this scenario, the softening features associated with the energy loss are in an energy range where the CR spectra are distorted by solar modulations. Understanding the (interstellar) shape of the spectra therefore requires a sufficiently good understanding of the solar modulation effects. In the present work we have shown, using a very simple model for the modulations, that the observations are possibly consistent with interstellar spectra that, in the regime $E \lesssim 30$ GeV, are unbroken power laws, in conflict with the hypothesis that the critical energy $E^*$ is in this energy range. Additional studies, based on more detailed modelings of solar modulations, are clearly needed to reach a more firm conclusion.

The alternative solution for the critical energy $E^*$ is to identify the softening associated with energy-loss effects

with the spectral break observed in the $(e^- + e^+)$ spectrum at $E \simeq 1$ TeV. This solution implies a much shorter CR residence time in the Galaxy, probably in conflict with models where the source of secondary nuclei is nuclear fragmentation in interstellar space.

An attractive consequence of this "high critical energy scenario" is that it provides a natural explanation for the intriguing result that the spectra of positrons and antiprotons have (in a broad energy interval from 30–400 GeV) approximately the same spectral index and a ratio $e^+/\bar{p} \simeq 2$, simply assuming that the dominant source for both antiparticles is secondary production. This is a straightforward consequence of the fact that in this energy range the propagation of positrons and antiprotons is approximately equal because the energy losses are small for both particles (even if the rates of energy loss differ by many orders of magnitude). An additional attractive feature of this solution for the critical energy is that it provides a natural, simple interpretation for the TeV break in the all-electron spectrum as the imprint of energy losses. If $E^*$ is below 10 GeV it is necessary to postulate a different mechanism as the origin of the spectral break around 1 TeV, and this is not a trivial task. The apparent narrowness of the observed spectral feature is a problem for all models that address the origin of this structure.

An important problem for the "high critical energy scenario" is that it requires source spectra of electrons and protons with very different shapes. If this is correct the consequences for the properties of the CR sources are clearly very important.

An additional prediction for the electron spectrum (and possibly also for the positron spectrum) is that at sufficiently high energy (when energy losses are important) the space-time volume of the source shrinks rapidly with $E$, and since (as predicted) the sources are pointlike, transient, astrophysical objects, the granularity of the sources should leave an observable signature for the angular and energy distributions. The minimum energy where the "source granularity effects" should become observable grows with $E^*$. The nonobservation of source granularity effects, and the measurement for the $(e^- + e^+)$ spectrum of a shape consistent with a simple power law above the break at 1 TeV (up to the highest energy where measurements are available), appears to be in serious tension (if not open conflict) with the hypothesis that the source of CR electrons is SN explosions, if one chooses for $E^*$ the low energy solution. The high critical energy scenario is consistent with the idea that SN are the source of electrons, but the evidence for the discreteness of the source should become observable soon.

The main conclusion of this discussion is that the question of when energy-loss effects become important for the propagation of electrons and positrons is of central importance for CR studies. Intimately connected to this question are the problems of understanding the physical mechanism that generates the break at TeV energy in the $(e^- + e^+)$ spectrum and the search for source granularity effects in the spectra of electrons and positron.

Several lines of investigation, both theoretical and experimental, promise to make progress toward a clarification of these problems.

(i) Extend the measurements of the (separate) positron and electron spectra to higher energy. If the $e^-$ and $e^+$ spectra have spectral breaks with a significantly different shape, the high critical energy scenarios could be excluded (and in the opposite case, reinforced).
(ii) Measure with precision the shape of the spectral break around 1 TeV. Understanding the origin of the discrepancies between different measurements in this energy range is very desirable.
(iii) Extend the measurements of the $(e^- + e^+)$ spectrum to as high an energy as possible, with the hope of identifying some of the sources.
(iv) Develop a better understanding of the solar modulation effects to confirm (or refute) the low critical energy scenario.
(v) Study the spectra of electrons and positrons in different regions of the Galaxy (interpreting the measurements of the diffuse gamma ray flux).
(vi) Construct better models for the propagation of CR in the Galaxy.

## ACKNOWLEDGMENTS

I am grateful to Pasquale Blasi, Carmelo Evoli, Stefano Gabici, Daniele Gaggero, Tom Gaisser, Dario Grasso, Philipp Mertsch, Andrew Strong, and Elena Orlando for discussions.

## APPENDIX: MULTIPLE COMPONENTS IN THE $e^\mp$ SPECTRA

A large number of models for the interpretation of the positron flux assume that the spectrum is formed by two components, generated by different mechanisms, and predict the existence of a hardening feature associated with the transition from a (low energy) regime dominated by one component to a (high energy) regime dominated by the second component.

As discussed in the main text, if one assumes that the critical energy is $E^* \lesssim 10$ GeV, the observations require the existence of a hard source of positrons, together with the standard mechanism of secondary production in the inelastic interactions of protons and nuclei.

It is straightforward that in this situation it is natural to expect that the spectrum contains a hardening feature. In the simplest possible situation, the two components can be described by power laws with different exponents:

TABLE V. Parameters of fits to the electron and positron spectra measured by AMS02.

| | Electrons | Positrons |
|---|---|---|
| $K$ [GeV m$^2$ s sr]$^{-1}$ | $0.40 \pm 0.02$ | $0.014 \pm 0.001$ |
| $\gamma_1$ | $4.26^{+0.15}_{-0.14}$ | $3.99^{+0.21}_{-0.18}$ |
| $\gamma_2$ | $3.07^{+0.06}_{-0.07}$ | $2.68^{+0.07}_{-0.08}$ |
| $E_{\rm cross}$ [GeV] | $24.2^{+7.3}_{-4.5}$ | $15.64^{+5.0}_{-2.9}$ |
| $\varepsilon$ [GeV] | $1.63 \pm 0.10$ | $1.09^{+0.12}_{-0.11}$ |
| $\chi^2_{\rm min}$ | 14.1 | 21.6 |
| $N_{\rm d.o.f.}$ | 65 | 64 |

$$\phi(E) = K_1 \left(\frac{E}{E_0}\right)^{-\gamma_1} + K_2 \left(\frac{E}{E_0}\right)^{-\gamma_2}. \tag{A1}$$

If $\gamma_1 > \gamma_2$, the first component has the softest spectrum and is dominant at low energy. The cross-over energy where the two components are equal is

$$E_{\rm cross} = E_0 \left(\frac{K_1}{K_2}\right)^{1/(\gamma_1-\gamma_2)} \tag{A2}$$

and the spectrum can also be expressed in the form

$$\phi(E) = K_1 \left(\frac{E}{E_0}\right)^{-\gamma_1} \left[1 + \left(\frac{E}{E_{\rm cross}}\right)^{-(\gamma_2-\gamma_1)}\right]. \tag{A3}$$

Comparing Eqs. (A3) and (3) one can see that the two model components are exactly described by the form of Eq. (3), when the width parameter has the value

$$w = \frac{1}{\gamma_1 - \gamma_2}. \tag{A4}$$

In fact, the widths of the best fits for positrons and electrons estimated in Sec. II are of the same order of $(\gamma_1 - \gamma_2)^{-1}$, and therefore it is interesting to verify if it is possible to describe the hardenings in the positron and electron spectra as the manifestations of the presence of two components. In order to do this, one can fit the observations using as a template the expression in Eq. (A3) distorted by solar modulations (described by the FFA algorithm), that is, with the five-parameter form:

$$\phi(E) = K_1 \frac{E^2}{(E+\varepsilon)^2} \left(\frac{E+\varepsilon}{E_0}\right)^{-\gamma_1} \left[1 + \left(\frac{E}{E_{\rm cross}}\right)^{-(\gamma_2-\gamma_1)}\right]. \tag{A5}$$

The results of fits performed on the basis of Eq. (A5) are given in Table V and are of good quality.

In the case of positrons the fit has $\chi^2_{\rm min} = 21.6$ (for 64 d.o.f.), only marginally worse ($\Delta\chi^2 \simeq 0.6$) than the more general fit performed with the model of Eq. (5), when in fact one has one less parameter. For the electron flux one has $\chi^2_{\rm min} = 14.1$ (for 65 d.o.f.). This has $\Delta\chi^2 \simeq 2.4$ with respect to the fit performed in the more general model where the width $w$ is a free parameter. The crossing energies for the best fits are $E_{\rm cross} \simeq 24.2^{+7.3}_{-4.5}$ for electrons and $E_{\rm cross} \simeq 15.6^{+5.0}_{-2.9}$ for positrons.

The crucial question is if the two components that emerge from this fit procedure are real or simply a mathematical artefact.

A reason to doubt that the hardening seen in the positron flux is associated with a new component is the fact that hardenings of similar structure are seen in both the $e^-$ and $e^+$ spectra. Most models for a new source of positrons (including acceleration from young pulsars and creation in dark matter particle self-annihilation or decay) predict that the new mechanism generates approximately equal source spectra of $e^-$ and $e^+$.

The hypothesis of a new hard component with equal contributions to the $e^-$ and $e^+$ spectra is, however, not consistent with the data. In the energy range 10–30 GeV, where the spectral hardenings are visible, the electron flux is more than 1 order of magnitude larger than the positron flux, and therefore the second (hard) component for electrons is much larger than the same component for positrons (see also Table V).

The existence of the hardening in the $e^-$ and $e^+$ spectra remains an intriguing feature, perhaps generated by propagation effects, that has not yet found a convincing explanation.


[1] O. Adriani *et al.* (PAMELA Collaboration), Phys. Rev. Lett. **106**, 201101 (2011).
[2] O. Adriani *et al.* (PAMELA Collaboration), Phys. Rev. Lett. **111**, 081102 (2013).
[3] O. Adriani *et al.*, Phys. Rep. **544**, 323 (2014).
[4] O. Adriani *et al.*, Astrophys. J. **810**, 142 (2015).
[5] O. Adriani *et al.*, Phys. Rev. Lett. **116**, 241105 (2016).
[6] M. Aguilar *et al.* (AMS Collaboration), Phys. Rev. Lett. **113**, 121102 (2014).
[7] M. Aguilar *et al.* (AMS Collaboration), Phys. Rev. Lett. **121**, 051102 (2018).
[8] L. J. Gleeson and W. I. Axford, Astrophys. J. **154**, 1011 (1968).
[9] P. Lipari, Astropart. Phys. **97**, 197 (2018).

[10] M. Potgieter, Living Rev. Solar Phys. **10**, 3 (2013).
[11] It can be noted that the $\chi^2$ per degree of freedom of the fit (of order 0.18) is small. This is the consequence of the existence of significant correlations between the systematic errors for the flux measurements at different energies. The same point can be made for the other fits to the data discussed in this paper. The relevant error correlation matrices have not been made public by the collaborations that performed the measurements.
[12] Treating the quantity $f$ as a nuisance parameter, including an additional term $(\delta f/\sigma_f)^2$ in the $\chi^2$ expression does not appreciably change the result of the fit.
[13] M. Aguilar *et al.* (AMS Collaboration), Phys. Rev. Lett. **113**, 221102 (2014).
[14] S. Abdollahi *et al.* (Fermi-LAT Collaboration), Phys. Rev. D **95**, 082007 (2017).
[15] J. Chang *et al.*, Nature (London) **456**, 362 (2008).
[16] O. Adriani *et al.* (CALET Collaboration), Phys. Rev. Lett. **119**, 181101 (2017).
[17] O. Adriani *et al.*, Phys. Rev. Lett. **120**, 261102 (2018).
[18] G. Ambrosi *et al.* (DAMPE Collaboration), Nature (London) **552**, 63 (2017).
[19] F. Aharonian *et al.* (HESS Collaboration), Phys. Rev. Lett. **101**, 261104 (2008).
[20] F. Aharonian *et al.* (HESS Collaboration), Astron. Astrophys. **508**, 561 (2009).
[21] D. Kerszberg (HESS Collaboration), in *Proceedings of the 35th ICRC* (2017), https://www.mpi-hd.mpg.de/hfm/HESS/pages/home/som/2017/09/.
[22] D. B. Tridon *et al.* (MAGIC Collaboration), arXiv:1110.4008.
[23] D. Staszak (VERITAS Collaboration), Proc. Sci. ICRC2015 (**2016**) 411.
[24] P. Lipari and S. Vernetto, Phys. Rev. D **98**, 043003 (2018).
[25] The use of the width parameter $w$ is preferable because it has a clear and intuitive physical meaning as the width of the spectral break. In this case (where $\Delta\gamma \simeq 1$) $s$ and $w$ are approximately the same, but in general, the two quantities can be very different.
[26] P. Morrison, S. Olbert, and B. Rossi, Phys. Rev. **94**, 440 (1954).
[27] V. L. Ginzburg and S. I. Syrovatskii, *The Origin of Cosmic Rays* (Pergamon Press, New York, 1964).
[28] In this work we only consider ultrarelativistic particles of unit electric charge, so that $p/|Z| \simeq E$, and for simplicity, we use the notation $D(E)$ for the diffusion coefficient (which depends on the absolute value of the rigidity and on the particle velocity $\beta$).
[29] P. Lipari, arXiv:1407.5223.
[30] D. R. Cox and H. D. Miller, *The Theory of Stochastic Processes* (Chapman and Hall, London, 1965).
[31] T. K. Gaisser, R. Engel, and E. Resconi, *Cosmic Rays and Particle Physics* (Cambridge University Press, Cambridge, England, 2016).
[32] D. Grasso *et al.* (Fermi-LAT Collaboration), Astropart. Phys. **32**, 140 (2009).
[33] G. L. Case and D. Bhattacharya, Astrophys. J. **504**, 761 (1998).
[34] I. Yusifov and I. Kucuk, Astron. Astrophys. **422**, 545 (2004).
[35] M. Garcia-Munoz, G. M. Mason, and J. A. Simpson, Astrophys. J. **217**, 859 (1977); S. P. Ahlen *et al.*, Astrophys. J. **534**, 757 (2000); N. E. Yanasak *et al.*, Astrophys. J. **563**, 768 (2001).
[36] R. Cowsik and B. Burch, Phys. Rev. D **82**, 023009 (2010).
[37] R. Cowsik, B. Burch, and T. Madziwa-Nussinov, Astrophys. J. **786**, 124 (2014).
[38] S. Abdollahi *et al.* (Fermi-LAT Collaboration), Phys. Rev. Lett. **118**, 091103 (2017).
[39] Y. S. Yoon *et al.*, Astrophys. J. **839**, 5 (2017).
[40] P. Lipari, Phys. Rev. D **95**, 063009 (2017).